European Biophysics Journal (2023) 52:153–173
https://doi.org/10.1007/s00249-023-01660-1

ORIGINAL ARTICLE

Mechanistic insights of neuronal calcium and IP_3 signaling system regulating ATP release during ischemia in progression of Alzheimer's disease

Anand Pawar[1] · **Kamal Raj Pardasani**[1]

Received: 5 December 2022 / Revised: 21 March 2023 / Accepted: 10 May 2023 / Published online: 24 May 2023

Abstract
The mechanisms of calcium ($[Ca^{2+}]$) signaling in various human cells have been widely analyzed by scientists due to its crucial role in human organs like the heartbeat, muscle contractions, bone activity, brain functionality, etc. No study is reported for interdependent $[Ca^{2+}]$ and IP_3 mechanics regulating the release of ATP in neuron cells during Ischemia in Alzheimer's disease advancement. In the present investigation, a finite element method (FEM) is framed to explore the interdependence of spatiotemporal $[Ca^{2+}]$ and IP_3 signaling mechanics and its role in ATP release during Ischemia as well as in the advancement of Alzheimer's disorder in neuron cells. The results provide us insights of the mutual spatiotemporal impacts of $[Ca^{2+}]$ and IP_3 mechanics as well as their contributions to ATP release during Ischemia in neuron cells. The results obtained for the mechanics of interdependent systems differ significantly from the results of simple independent system mechanics and provide new information about the processes of the two systems. From this study, it is concluded that neuronal disorders cannot only be simply attributed to the disturbance caused directly in the processes of calcium signaling mechanics, but also to the disturbances caused in IP_3 regulation mechanisms impacting the calcium regulation in the neuron cell and ATP release.

Keywords Calcium and IP_3 mechanics · ATP release · Finite element method · Ischemia · Alzheimer's disease

Introduction

Inspite of the development of high throughput technology and the generation of a large volume of data and advancement in computer sciences, scientists have not been able to discover and develop proper protocols for the diagnosis and cure of neuronal diseases including Alzheimer's, Parkinson's, Ischemia, etc. Calcium, IP_3, ATP, etc. are reported to have roles in these neuronal disorders. The experimentalists and computational neuroscientists are very actively investigating the $[Ca^{2+}]$ signaling mechanisms in neurons to address the issues of neuronal disorders. Calcium not only plays a significant role in neuronal signaling but also has crucial roles in human cells like astrocytes, myocytes, Oocytes, etc.

The mathematics of diffusion in a plane sheet, cylinder, and sphere with constant and concentration-dependent diffusion coefficients has been discussed by Crank (1979). Llinas (1979) developed a comprehensive mathematical model for synaptic transmission and explained the function of calcium as a regulator of the cell's biological properties such as hormone release as well as dendroplasmic flow and genome expression in neuron cells. Rasmussen and Barrett (1984) explored the integrated view of the calcium signaling system in the light of calcium receptor protein, cellular $[Ca^{2+}]$ metabolism, biochemical events, calcium cycling, etc. Fogelson and Zucker (1985) explored the presynaptic calcium transport model with cytoplasmic binding for a one-dimensional case. They also explained the extrusion of calcium by the process of pump and influx from different arrays of single channels. Ahmed and Connor (1988) examined the determination of calcium buffer in the capacity of the cytoplasm utilizing measured EGTA amount in molluscan neurons during calcium transients. The different $[Ca^{2+}]$ signaling events including $[Ca^{2+}]$ release, $[Ca^{2+}]$ entry, etc.

✉ Anand Pawar
ap.193104003@manit.ac.in

Kamal Raj Pardasani
kamalrajp@rediffmail.com

[1] Department of Mathematics, Bioinformatics and Computer Applications, Maulana Azad National Institute of Technology, Bhopal, Madhya Pradesh 462003, India

with respective channels in various tissues were explored by Bootman and Berridge (1995). Wagner and Keizer (1994) and Smith et al. (1996) devised a [Ca^{2+}] transport model involving buffer and explored the conditions which validate the buffer approximations for calcium channels. The high amounts of slow buffers can cause the oscillatory behavior of calcium concentration (Falcke 2003) since slow buffers allow excess amounts of calcium release and bind more calcium ions. The neuronal endoplasmic reticulum operates the diverse signaling events and [Ca^{2+}] release from ER, which is associated with numerous intracellular processes (Verkhratsky 2002) and diverse neuronal pathologies (Brini et al. 2014). Several researchers have explored the [Ca^{2+}] signaling since last ten years in several cells like astrocyte (Jha et al. 2013, 2014), neuron cell (Tewari and Pardasani 2010, 2012; Tripathi and Adlakha 2011, 2012; Jha and Adlakha 2015), acinar cell (Manhas et al. 2014; Manhas and Pardasani 2014; Manhas and Anbazhagan 2021), fibroblast cells (Kotwani et al. 2012, 2014), Oocytes (Panday and Pardasani 2013; Naik and Pardasani 2015, 2016, 2019), myocyte (Pathak and Adlakha 2015, 2016) and hepatocyte cells (Jagtap and Adlakha 2018), etc. utilizing several numerical and analytical procedures. Tewari et al. (2011) have discussed the [Ca^{2+}] transport model integrating ion channels, sodium-calcium exchanger (NCX) and sarcolemmal [Ca^{2+}] ATPase pump with the excess buffering mechanism in neurons. Tripathi and Adlakha (2012) explored the two-dimensional calcium diffusion model involving diffusion rate, buffer, potential activities and influxes to have an understanding of chemical signaling mechanisms in neuron cells. Jha and Adlakha (2015) explored the neuronal calcium transport model analytically involving buffer, diffusion coefficient and flux effects for two-dimensional unsteady cases utilizing Laplace transform. The calcium distribution with the sodium–calcium exchanger, calcium-binding buffer, and voltage-gated calcium channels (VGCC) for Alzheimer's-affected neuron cells has been explored by Dave and Jha (2021).

The relationship between PIP_2 catabolism and a rise in intracellular [Ca^{2+}] has been hypothesized by Michell (1975). The phosphatidylinositol 4, 5-bisphosphate hydrolyzes and produces IP_3 and also diacylglycerol by the signal transduction process (Berridge and Irvine 1984). The IP_3 plays a functional role in releasing [Ca^{2+}] from internal stores and coordinates numerous processes such as neuronal signaling, transformation, fertilization, cell growth, muscle contraction, apoptosis, transcriptional activation and cell differentiation (Berridge et al. 2000). The bistability of calcium and IP_3 dynamics is established by IP_3-mediated [Ca^{2+}] release and [Ca^{2+}]-mediated IP_3 generation. The ryanodine (RyR) and IP_3-gated channels (IP_3R) display the bell-shaped curves for their dependence on [Ca^{2+}] as reported by Bezprozvanny et al. (1991). For having an understanding of the fundamentals of IP_3 and [Ca^{2+}] signaling, Allbritton et al. (1992) discussed the messenger actions of IP_3 and [Ca^{2+}] and measured their diffusion coefficients in cells. The oscillations in calcium concentration have been identified on the basis of inhibition and activation of IP_3 channels in the ER through voltage-gated [Ca^{2+}] and potassium (K^+) channels by Keizer and De Young (1993). The minimal model of cytosolic calcium fluctuations by calcium release due to the IP_3 receptor (IP_3R) which is modulated by calcium signaling in a biphasic process (Atri et al. 1993) is reported in the past. Li and Rinzel (1994) explored the two-variable systems for [Ca^{2+}] oscillations which are mediated by IP_3 receptor channels in the ER by reducing the Young Keizer model. Falcke et al. (2000) explained the function of calcium with IP_3 in the generation of regular fluctuations as well as chaotic behavior in neuron cells. Wagner et al. (2004) explained that [Ca^{2+}] regulates the generation of IP_3 concentration, which further fertilizes the [Ca^{2+}] wave propagation in Xenopus eggs. Recently, the calcium and IP_3 signaling have been explored in different cells including myocyte cells (Singh and Adlakha 2019; 2020), hepatocyte cells (Jagtap and Adlakha 2019) and neuron cells (Pawar and Pardasani 2022a, d) by utilizing different numerical procedures.

The failure of calcium homeostasis is reported with the Ischemic brain damage (Siesjö 1984). The ischemic conditions are accompanied by the accumulation of calcium causing irreversible damage to the cells (Yanagihara and John 1982; Deshpande et al. 1987). The influx of extracellular [Ca^{2+}] through different types of channels including VGCC, NCX etc. elevates the cytosolic [Ca^{2+}] concentration, which may cause the neurotoxicity and Ischemic neuronal injury (Choi 1988). The aberrant [Ca^{2+}] release from ER via IP_3 (Mattson et al. 2000) and ryanodine receptors (Bull et al. 2008; Ruiz et al. 2009) and impaired extrusion of cytosolic [Ca^{2+}] by the SERCA pump to ER (Stutzmann and Mattson 2011) can cause the elevation in [Ca^{2+}] levels during Ischemia (Bodalia et al. 2013). The depletion of ATP is more rapid in the case of Ischemia. The dysregulation in the ER mechanism during Ischemia can cause neuronal injury which may further lead to cell death. The elevated calcium levels in cells are linked with Ischemic Stroke (Chung et al. 2015). Wojda et al. (2008) discussed the neuronal pathologies in which the dysregulation of calcium homeostasis including [Ca^{2+}] influx, impaired [Ca^{2+}] extrusion, etc. can cause brain injury or Ischemia which may lead to rapid neuronal death. The massive release of ATP is correlated with the Ischemia condition and is responsible for different neurodegenerative diseases (Volonté et al. 2003). The ATP release in response to the elevation of intracellular calcium levels during Ischemia quickly hydrolyzes the adenosine through ectonucleotidases and elevation in the extracellular adenosine is associated with Ischemic conditions (Rossi et al. 2007). The contribution of [Ca^{2+}] pumps, calcium

buffering systems, intracellular calcium stores, calcium-permeable ionic channels, calcium-dependent processes etc. in the nervous system during Ischemia was explored by Tymianski and Tator (1996). Kalaria (2000) explored the various factors and pathophysiology having the association with Ischemia and Alzheimer's disease as Ischemia notably increases the risk for Alzheimer's disease progression. Alzheimer's is at high risk for Ischemic events in nerve cells since brain Ischemia contributes to Alzheimer's disorder pathogenesis (Koistinaho and Koistinaho 2005). Stamatakis and Mantzaris (2006) studied the mathematical model with ATP-mediated IP_3 generation, calcium release from ER via IP_3 receptor, ATP release, etc. to explore the calcium-dependent and IP_3-dependent ATP release mechanisms in the nervous system. Pluta et al. (2013) discussed that brain ischemia alters the Alzheimer's-related genes which compromise nerve functions and cause advanced sporadic Alzheimer's disorder. Brain Ischemia is the cause of the initiation of Alzheimer's disorders since the post-ischemic brain alterations are linked with the accumulation of unfolding proteins including tau-protein, β-amyloid etc. which are Alzheimer's-related proteins (Pluta et al. 2021). Pawar and Pardasani (2022b, c, 2023) explored the dysregulation in different mechanisms of $[Ca^{2+}]$ with nitric oxide, β-amyloid and dopamine, which are linked with several neuronal illnesses including Alzheimer's, Parkinson's diseases. In the literature survey, it was pointed out by various studies that calcium levels and ATP release are higher in Ischemic neuron cells, but what events lead to such higher calcium and IP_3 concentrations and higher amounts of the release of ATP during Ischemia are not clearly understood till date. Thus, the present study is focused on exploring such events by the proposed model.

The previous models did not explore the effects of sodium-calcium exchanger, VGCC and $[Ca^{2+}]$-induced calcium release (CICR) through the RyR on the interdependent $[Ca^{2+}]$ and IP_3 dynamics in neurons. The regulation of ATP release through interdependent $[Ca^{2+}]$ and IP_3 neurodynamics incorporating different parameters like buffer, SERCA pump, IP_3R, RyR, VGCC and NCX has not been investigated earlier in neuron cells. Also, the systems dynamics of interdependent $[Ca^{2+}]$ and IP_3 with the association of different crucial parameters regulating ATP release in disease-associated neuron cells like Ischemic neurons were not studied earlier. In the present study, a one-dimensional model of interdependent $[Ca^{2+}]$ and IP_3 dynamics regulating ATP release in normal and ischemic neurons has been proposed incorporating the parameters like buffer, SERCA pump, IP_3-receptor, ryanodine receptor, VGCC and NCX. The two-way feedback between $[Ca^{2+}]$ and IP_3 and one-way feedback from $[Ca^{2+}]$ and IP_3 to ATP release are incorporated in the present model. The model is framed in the form of the initial boundary value problem incorporating the system of reaction–diffusion equations for calcium and IP_3 dynamics in neuron cells. The FEM was utilized to get the outcomes and, the effects of the several parameters on the interdependent $[Ca^{2+}]$ and IP_3 mechanisms in ATP release regulation during Ischemia and Alzheimer's in neurons have been explored.

Mathematical formulation

In neuron cells, the $[Ca^{2+}]$ kinetics is determined by the set of reaction–diffusion equations, which can be formulated considering the bimolecular reactions between $[Ca^{2+}]$ and buffer species as follows (Smith 1996),

$$[Ca^{2+}] + [B_j] \underset{k_j^-}{\overset{k_j^+}{\leftrightarrow}} [CaB_j] \tag{1}$$

where, $[Ca^{2+}]$, $[B_j]$ and $[CaB_j]$ are, respectively, depicting the cytosolic calcium, free buffer and calcium bound buffer concentrations. For buffer 'j', the association and dissociation rates are sequentially denoted by K_j^+ and K_j^-. The resulting PDE's in one-dimensional case for Eq. (1) by utilizing Fickian diffusion (Smith 1996) can be represented as,

$$\frac{\partial [Ca^{2+}]}{\partial t} = D_{Ca} \nabla^2 [Ca^{2+}] + \sum_j R_j \tag{2}$$

$$\frac{\partial [B_j]}{\partial t} = D_{B_j} \nabla^2 [B_j] + R_j \tag{3}$$

$$\frac{\partial [CaB_j]}{\partial t} = D_{CaB_j} \nabla^2 [CaB_j] - R_j \tag{4}$$

where,

$$R_j = -K_j^+ [B_j][Ca^{2+}] + K_j^- [CaB_j] \tag{5}$$

D_{Ca}, D_{Bj} and D_{CaBj} are, respectively, representing the diffusion coefficient of calcium, free buffer and $[Ca^{2+}]$ bound buffer. For stationary, fixed or immobile buffer, $D_{Bj} = D_{CaBj} = 0$. The obtained Eqs. (2–5) are simplified as (Smith 1996),

$$\frac{\partial [Ca^{2+}]}{\partial t} = D_{Ca} \nabla^2 [Ca^{2+}] - K^+ [B]_\infty \left([Ca^{2+}] - [Ca^{2+}]_\infty \right) \tag{6}$$

Incorporating EGTA buffer concentration, ryanodine channel with VGCC and NCX in the Wagner et al. (2004) model for calcium and IP_3 distributions for a one-dimensional case can be expressed in neurons as,

$$\frac{\partial [Ca^{2+}]}{\partial t} = D_{Ca} \frac{\partial^2 [Ca^{2+}]}{\partial x^2} + \left(\frac{J_{IPR} - J_{SERCA} + J_{LEAK} + J_{RyR}}{F_C} \right) - K^+ [B]_\infty \left([Ca^{2+}] - [Ca^{2+}]_\infty \right) + J_{VGCC}. \tag{7}$$

Here, the steady-state concentrations for buffer and $[Ca^{2+}]$ are, respectively, symbolized by $[B]_\infty$ and $[Ca^{2+}]_\infty$. The terms x and t are, respectively, location and time parameters. For $[Ca^{2+}]$, the temporal and spatial domains are correspondingly $t > 0$ and $0 \le x \le 5\ \mu m$.

The various terms of influx and outflux in Eq. (7) are given by Wagner et al. (2004) and IP_3 receptor terms are given by Li and Rinzel (1994),

$$J_{IPR} = V_{IPR} m^3 h^3 \left([Ca^{2+}]_{ER} - [Ca^{2+}] \right) \tag{8}$$

$$J_{SERCA} = V_{SERCA} \left(\frac{[Ca^{2+}]^2}{[Ca^{2+}]^2 + K^2_{SERCA}} \right) \tag{9}$$

$$J_{LEAK} = V_{LEAK} \left([Ca^{2+}]_{ER} - [Ca^{2+}] \right) \tag{10}$$

$$J_{RyR} = P_0 V_{RyR} \left([Ca^{2+}]_{ER} - [Ca^{2+}] \right) \tag{11}$$

where, J_{IPR}, J_{SERCA}, J_{LEAK} and J_{RyR} are, respectively, the fluxes of the IP_3 receptor, SERCA pump, leak pump and ryanodine receptor. V_{LEAK}, V_{IPR} and V_{RyR} are sequentially the flux rate constants for Leak, IP_3R and ryanodine receptor. The rate and Michaelis constants for the SERCA pump are, respectively, V_{SERCA} and K_{SERCA}.

Li and Rinzel (1994) proposed the following expressions for m and h variables in Eq. (8),

$$m = \left(\frac{[IP_3]}{[IP_3] + K_{IP3}} \right) \left(\frac{[Ca^{2+}]}{[Ca^{2+}] + K_{Ac}} \right) \tag{12}$$

$$h = \frac{K_{Inh}}{K_{Inh} + [Ca^{2+}]} \tag{13}$$

where, for binding positions of activating IP_3, activating $[Ca^{2+}]$ and inhibiting $[Ca^{2+}]$, the dissociation constants are denoted sequentially by K_{IP3}, K_{Ac} and K_{inh}. J_{VGCC} is the flux of the VGCC, which is modeled by utilizing the Goldman–Hodgkin–Kartz (GHK) current equation as follows (Keener and Sneyd 2009),

$$I_{Ca} = P_{Ca} Z^2_{Ca} \frac{F^2 V_m}{RT} \frac{[Ca^{2+}]_i - [Ca^{2+}]_0 \exp\left(-Z_{Ca} \frac{FV_m}{RT}\right)}{1 - \exp\left(-Z_{Ca} \frac{FV_m}{RT}\right)} \tag{14}$$

where, the intracellular and extracellular $[Ca^{2+}]$ concentrations are depicted, respectively, by $[Ca^{2+}]_i$ and $[Ca^{2+}]_0$. The permeability and valency of calcium ions are denoted by P_{Ca} and Z_{Ca} correspondingly. F and V_m are, respectively, the Faradays constant and membrane potential. The real gas constant and absolute temperature are denoted by R and T sequentially. Equation (14) is transformed into the molar/sec by utilizing following equation as shown below,

$$J_{VGCC} = -\frac{I_{Ca}}{Z_{Ca} F V_{cytosol}} \tag{15}$$

The equation of GHK current, which is derived from the constant field, provides the current density as a voltage function. Also, the neuronal calcium ions are regulated by the $Na^+/[Ca^{2+}]$ exchanges (NCX) by exchanging one $[Ca^{2+}]$ ion with three Na^+ ions. The regulation of calcium ions through NCX is expressed as follows (Nelson and Cox 2005; Tewari and Pardasani 2008; Panday and Pardasani 2013),

$$\sigma_{NCX} = Ca_0 \left(\frac{Na_i}{Na_0} \right)^3 \exp\left(\frac{FV_m}{RT} \right) \tag{16}$$

where, Na_i and Na_0 are, respectively, depicting the intracellular and extracellular sodium concentration.

Here IP_3 dynamics involving $[Ca^{2+}]$ deduced by Wagner et al. (2004) is utilized and thus IP_3 distribution with $[Ca^{2+}]$ can be represented in neurons as,

$$\frac{\partial [IP_3]}{\partial t} = D_i \frac{\partial^2 [IP_3]}{\partial x^2} + \frac{J_{production} - \lambda \left(J_{kinase} + J_{phosphatase} \right)}{F_c} \tag{17}$$

where, D_i denotes the IP_3 diffusion coefficient. The spatial and temporal domains for IP_3 are $0 \le x \le 5\ \mu m$ and $t > 0$, respectively.

The IP_3 concentration is represented by $[IP_3]$. Wagner et al. (2004) provided the $[Ca^{2+}]$-dependent formation of IP_3 as expressed below:

$$J_{production} = V_{production} \left(\frac{[Ca^{2+}]^2}{[Ca^{2+}]^2 + K^2_{production}} \right) \tag{18}$$

The expressions for IP_3 degradation by J_{Kinase} and $J_{phosphatase}$ are provided by Sims and Allbrittont (1998) and Bugrim et al. (2003), which are given below:

$$J_{kinase} = (1 - \zeta) V_1 \left(\frac{[IP_3]}{[IP_3] + 2.5} \right) + \zeta V_2 \left(\frac{[IP_3]}{[IP_3] + 0.5} \right) \tag{19}$$

$$J_{phosphatase} = V_{ph} \left(\frac{[IP_3]}{[IP_3] + 30} \right) \tag{20}$$

$$\zeta = \left(\frac{[Ca^{2+}]}{[Ca^{2+}] + 0.39} \right) \tag{21}$$

where, $J_{Production}$ is the flux term for IP_3 production. Also, J_{Kinase} and $J_{Phosphatase}$ are the flux terms for IP_3 degradation.

Here, the maximum IP_3 generation rate is $V_{Production}$ and Michaelis constant for $[Ca^{2+}]$ activation is $K_{Production}$. V_1 and V_2 are, respectively, the rate constants for low and high $[Ca^{2+}]$ (3-kinase). V_{ph} denotes the rate constant for phosphatase. The adjustable parameter λ is used to approximate the elimination rate. The $[Ca^{2+}]_{ER}$ can be estimated utilizing the total cellular $[Ca^{2+}]$ conservation relationship,

$$[Ca^{2+}]_T = F_E\,[Ca^{2+}]_{ER} + F_C\,[Ca^{2+}]_C \tag{22}$$

Initial conditions

It is considered that the neuron cell is at rest at time t = 0 and maintains background concentration. Smith (1996), Tewari and Pardasani (2010) and Fink et al. (2000), Brown et al. (2008), respectively, proposed the initial concentrations for $[Ca^{2+}]$ and IP_3 as expressed below,

$$\left[Ca^{2+}\right]_{t=0} = 0.1\,\mu M \tag{23}$$

$$\left[IP_3\right]_{t=0} = 0.16\,\mu M \tag{24}$$

Boundary conditions

For $[Ca^{2+}]$, the boundary condition is given by (Smith 1996; Tewari and Pardasani 2010),

$$\lim_{x\to 0}\left(-D_{ca}\frac{\partial\left[Ca^{2+}\right]}{\partial x}\right) = \sigma_{Ca} - \sigma_{NCX} \tag{25}$$

where, σ_{Ca} represents calcium source influx.

At the boundary distant from source location, $[Ca^{2+}]$ reaches the concentration of 0.1 μM (Smith 1996; Tewari and Pardasani 2010),

$$\lim_{x\to 5}\left[Ca^{2+}\right] = \left[Ca^{2+}\right]_{\infty} = 0.1\mu M \tag{26}$$

The boundary concentrations for IP_3 dynamics as provided by Fink et al. (2000) and Brown et al. (2008) are utilized and shown below,

$$\lim_{x\to 5}\left[IP_3\right] = 0.16\,\mu M \tag{27}$$

$$\lim_{x\to 0}\left[IP_3\right] = 3\mu M, t > 0; \tag{28}$$

The calcium-dependent and IP_3-dependent ATP release is given by Stamatakis and Mantzaris (2006) as,

$$J_{RELEASE} = \beta\,F_1\left(\left[Ca^{2+}\right]\right)\,F_2\left(IP_3\right) \tag{29}$$

where, β is the maximum production rate and $F_1([Ca^{2+}])$ and $F_2(IP_3)$ are the $[Ca^{2+}]$-dependent and IP_3-dependent ATP release, respectively.

The $[Ca^{2+}]$-dependent and IP_3-dependent ATP release are defined as (Stamatakis and Mantzaris 2006),

$$F_1\left(\left[Ca^{2+}\right]\right) = \left(\frac{\left(\frac{f_0}{f_0-1}\right) - 2\left(\frac{[Ca^{2+}]}{[Ca^{2+}]_{max}}\right)}{\left(\frac{1}{f_0-1}\right) - \left(\frac{[Ca^{2+}]}{[Ca^{2+}]_{max}}\right)^2}\right) \tag{30}$$

$$F_2\left(IP_3\right) = \left(\frac{\left(\frac{g_0}{g_0-1}\right) - 2\left(\frac{IP_3}{(IP_3)_{max}}\right)}{\left(\frac{1}{g_0-1}\right) - \left(\frac{IP_3}{(IP_3)_{max}}\right)^2}\right) \tag{31}$$

where, f_0 and g_0 are the constants for ATP feedback and $[Ca^{2+}]_{max}$ and $[IP_3]_{max}$ are the considered maximum values of calcium and IP_3 in cells. The finite element technique has been utilized for solving the equations system for $[Ca^{2+}]$ and IP_3 in the regulation of ATP release in neuron cells as exhibited in the Appendix.

Results and discussion

The obtained outcomes for $[Ca^{2+}]$ and IP_3 equations are exhibited graphically to understand the impacts of several parameters like buffer concentration, SERCA pump, source amplitude, IP_3 receptor, ryanodine receptor, etc. on the interdependence of $[Ca^{2+}]$ and IP_3 signaling mechanisms with ATP release in Ischemia-affected nerve cells. The different parameters with numerical values and units are depicted below in Table 1.

Figure 1A displays spatial $[Ca^{2+}]$ distribution with VGCC and NCX in a neuron cell at various times t = 0.02, 0.05, 0.1 and 2.5 s. The calcium concentration falls down with the distant site from $x = 0$ up to 5.0 μm and approaches the framework concentration level. The $[Ca^{2+}]$ diffusion from the source to the opposite end of cells, fixing of free $[Ca^{2+}]$ by the buffer and the expulsion of cytosolic $[Ca^{2+}]$ to ER by the pump reduce the $[Ca^{2+}]$ in nerve cells. Figure 1B shows temporal $[Ca^{2+}]$ distribution at various sites in neurons. The neuronal $[Ca^{2+}]$ concentration rises as time increases at various sites due to the release of $[Ca^{2+}]$ ions upon the initiation of the source channel. The elevation in $[Ca^{2+}]$ concentration is noted from t = 0 up to 0.5 s and later it approaches the steady-state at different sites in cells.

Figure 2 depicts the ATP release which is considered as $[Ca^{2+}]$-dependent for different times and sites. The impact of $[Ca^{2+}]$ concentration on ATP release is significant. At the position where $[Ca^{2+}]$ concentration is more elevated, the ATP release is also elevated in Ischemia-affected neuron

Table 1 Numerical data

Symbols	Values	Reference	Symbols	Values	Reference
K_{serca}	0.4 μM	Wagner et al. (2004)	K_{IP3}	0.15 μM	Wagner et al. (2004)
V_{Leak}	0.01 s^{-1}	Wagner et al. (2004)	V_{IPR}	8.5 s^{-1}	Wagner et al. (2004)
V_{serca}	0.65 μM/s	Wagner et al. (2004)	K_{Ac}	0.8 μM	Wagner et al. (2004)
K_{inh}	1.8 μM	Wagner et al. (2004)	D_i	283 $\mu m^2 s^{-1}$	Wagner et al. (2004)
D_{Ca}	16 $\mu m^2 s^{-1}$	Wagner et al. (2004)	$K_{Production}$	0.4 μM	Wagner et al. (2004)
$V_{Production}$	0.075 $\mu M s^{-1}$	Wagner et al. (2004)	V_2	0.005 $\mu M s^{-1}$	Wagner et al. (2004)
V_1	0.001 $\mu M s^{-1}$	Wagner et al. (2004)	λ	30	Wagner et al. (2004)
V_{ph}	0.02 $\mu M s^{-1}$	Wagner et al. (2004)	F_E	0.17	Wagner et al. (2004)
F_C	0.83	Wagner et al. (2004)	g_0	0.05	Stamatakis and Mantzaris (2006)
f_0	0.05	Stamatakis and Mantzaris (2006)	k^+	1.5 $\mu M^{-1} s^{-1}$	Smith et al. (1996)
β	5 $\mu M s^{-1}$	Stamatakis and Mantzaris (2006)	V_{RyR}	0.5 μM/s	Naik and Pardasani (2015)
Z_{Ca}	2	Tewari and Pardasani (2008)	P_{Ca}	4.3×10^{-8} ms^{-1}	Naik and Pardasani (2015)
V_m	− 0.05 V	Naik and Pardasani (2015)	F	96,486 C/mol	Tewari and Pardasani (2008)
T	300 K	Naik and Pardasani (2015)	R	8.31 J/(molK)	Tewari and Pardasani (2008)
$V_{cytosol}$	523.6 μm^3	Tewari and Pardasani (2008)	$[Ca^{2+}]_0$	3 mM	Naik and Pardasani (2015)
Na_0	145 mM	Tewari and Pardasani (2008)	Na_i	20 mM	Naik and Pardasani (2015)

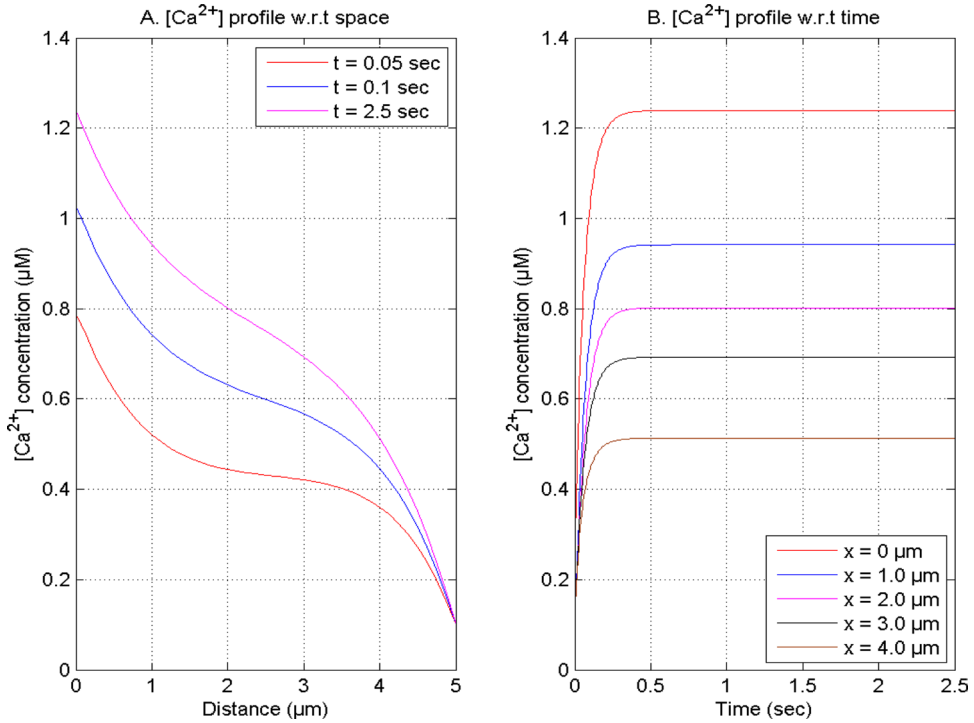

Fig. 1 $[Ca^{2+}]$ distribution in the presence of VGCC and NCX for σ = 15 pA and [B] = 5 μM at various times and sites

cells. The $[Ca^{2+}]$ concentration is generally high at location of the source ($x = 0$ μm) and the ATP release is also high at $x = 0$ μm. In Fig. 1A, the $[Ca^{2+}]$ reaches the steady-state in time 0.5 s and in Fig. 2A, the ATP release also achieves the equilibrium in time 0.5 s. The behavior of the curves is dominated by the boundary conditions near the boundary. Therefore, the behavior of the curves near the boundary of the cell is almost linear. The nonlinearity in behavior is observed far from the boundaries towards the center of the cell, where the processes are not in balance with each other and are undergoing adjustment to regulate the calcium concentration and ATP release according to the requirements of the cell. These adjustments are taking place between the $[Ca^{2+}]$ elevating and $[Ca^{2+}]$ reducing mechanisms, which are just both opposite and are pulling down each other. In Fig. 2A, the nonlinear behavior of $[Ca^{2+}]$-dependent ATP

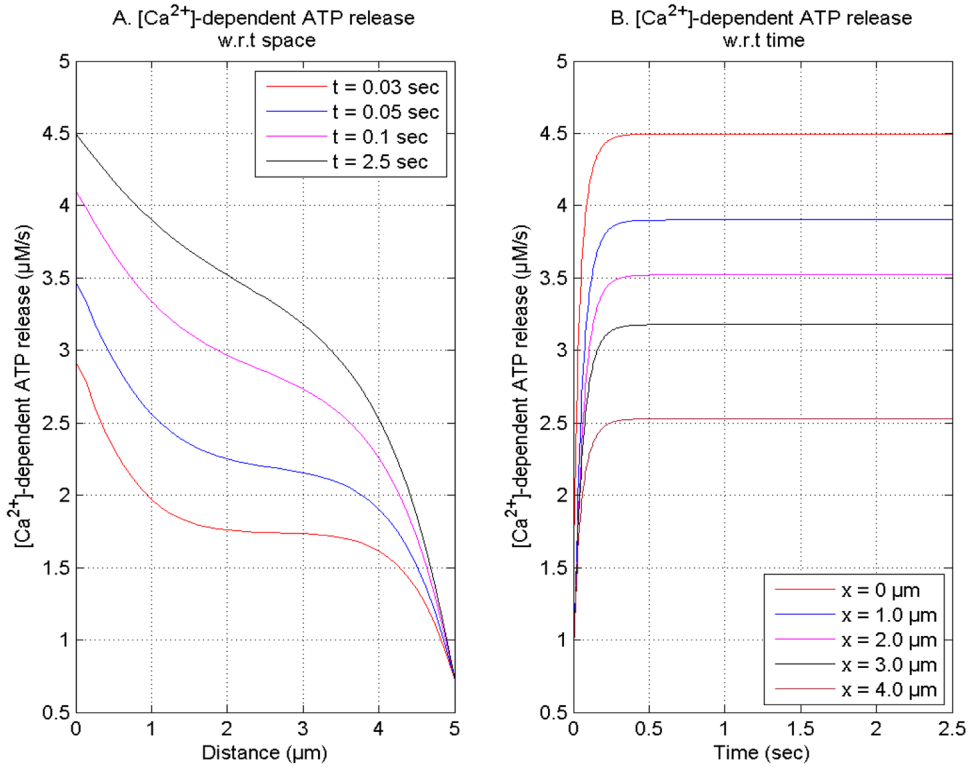

Fig. 2 $[Ca^{2+}]$-dependent ATP release in the presence of VGCC and NCX for $\sigma = 15$ pA and $[B] = 5$ μM at various times and locations

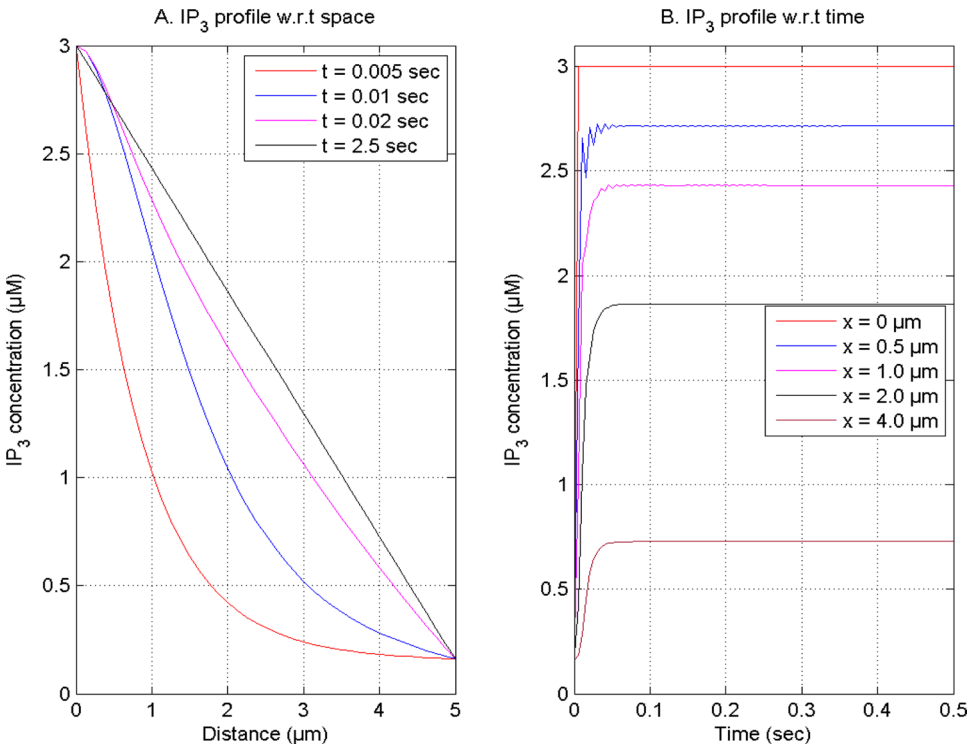

Fig. 3 IP_3 distribution in the presence of VGCC and NCX for $\sigma = 15$ pA & $[B] = 5$ μM at various times and positions

release approaches towards linearity with time due to the adjustment in different processes of calcium ions in neurons. This implies that the ATP release directly depends on $[Ca^{2+}]$ in neuron cells.

Figure 3A exhibits the spatial IP_3 ions distribution at different times in neuron cells. The IP_3 concentrations increase as we move away from the IP_3 source because IP_3 molecules near IP_3R bind together to balance the boundary

concentration of 3 µM for various times 0.005, 0.01, 0.02 and 0.5 s. Figure 3B exhibits the temporal IP_3 distribution at various locations $x = 0$, 0.5, 1.0, 2.0 and 4.0 µm in neuron cells. As time increases, IP_3 concentration rises quickly since the IP_3 stores near IP_3R bind with it to open it and release cytosolic $[Ca^{2+}]$ from the ER in neurons during Ischemia. Also, the reason for the changes in the behavior of the curves was mentioned in the discussion of Fig. 2 as the different processes of IP_3 dynamics achieve the equilibrium with time, which causes changes in the nonlinear behavior of IP_3 molecules as depicted in Fig. 3A in neurons.

Figure 4 shows the IP_3-dependent ATP release for distinct times and locations. The elevation in IP_3 levels can cause the elevation in IP_3-dependent ATP release in neuron cells. In Fig. 3A, it was seen that IP_3 is highest at $x = 0$ µm and falls down from location $x = 0$ µm up to $x = 5$ µm. Similarly, in Fig. 4A, the ATP release is highest at $x = 0$ µm and falls down with distant sites from $x = 0$ up to 5 µm corresponding to the decrease in IP_3 concentrations from site $x = 0$ up to 5 µm. As mentioned in the discussion of Fig. 2, the nonlinearity in the IP_3-dependent ATP release also reduces with time since the different mechanisms of IP_3 signaling approach the equilibrium state with time in neurons as illustrated in Fig. 4A. This confirms the direct relationship between ATP release and IP_3 concentration. The same correlations are observed in Figs. 3B and 4B for the temporal profile of IP_3 and ATP release, that is IP_3 and ATP release profiles achieve steady-state at the same time.

The computation has been carried out for varying buffer amounts in the range [5, 40] with VGCC and NCX in neurons. The consequences of buffering mechanism on $[Ca^{2+}]$ distribution in neuron cells concerning time for various buffer concentrations, i.e., [B] = 5, 10, 20, 40 µM is displayed in Fig. 5. With the increase in buffer amounts at time 2.5 s and location 0 µm, the neuronal $[Ca^{2+}]$ levels reduces. Since the buffer fixes additional $[Ca^{2+}]$ and thus causes the decrease in the free $[Ca^{2+}]$ in neuron cells. The dysregulation in the buffer mechanism causes an elevation in $[Ca^{2+}]$ concentration during Ischemia in neurons.

The consequences of the buffer mechanism on $[Ca^{2+}]$ distribution are seen in Fig. 5. In Figs. 5 and 6, the $[Ca^{2+}]$ concentration and ATP release decrease with the addition of buffer amounts. This implies that the influence of buffer on $[Ca^{2+}]$ is transferred to the ATP release in the same ratio of magnitude in neurons.

Figure 7 illustrates the temporal $[Ca^{2+}]$ distribution and $[Ca^{2+}]$-dependent ATP release at location $x = 0$ µm for various buffer amounts. It is seen that the calcium oscillations become larger in the initial period with the elevation in buffer amounts. The reason behind this is that when the buffer concentration is high, it fixes more $[Ca^{2+}]$ ions reducing free calcium in the cell and the other processes which are involved in raising calcium concentration compete with the buffer mechanism to make the calcium profile steady at a constant level. Both Fig. 7A, B indicate stable dynamics of $[Ca^{2+}]$ and ATP in the cell under present conditions.

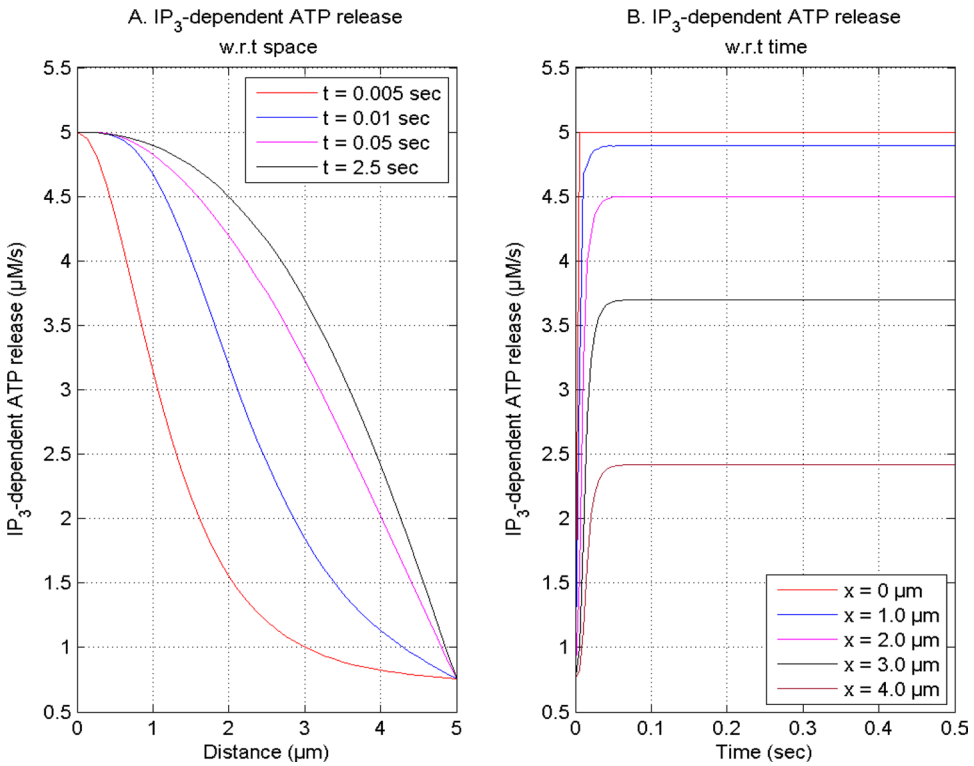

Fig. 4 IP_3-dependent ATP release with VGCC, NCX, σ = 15 pA & [B] = 5 µM at various times and sites

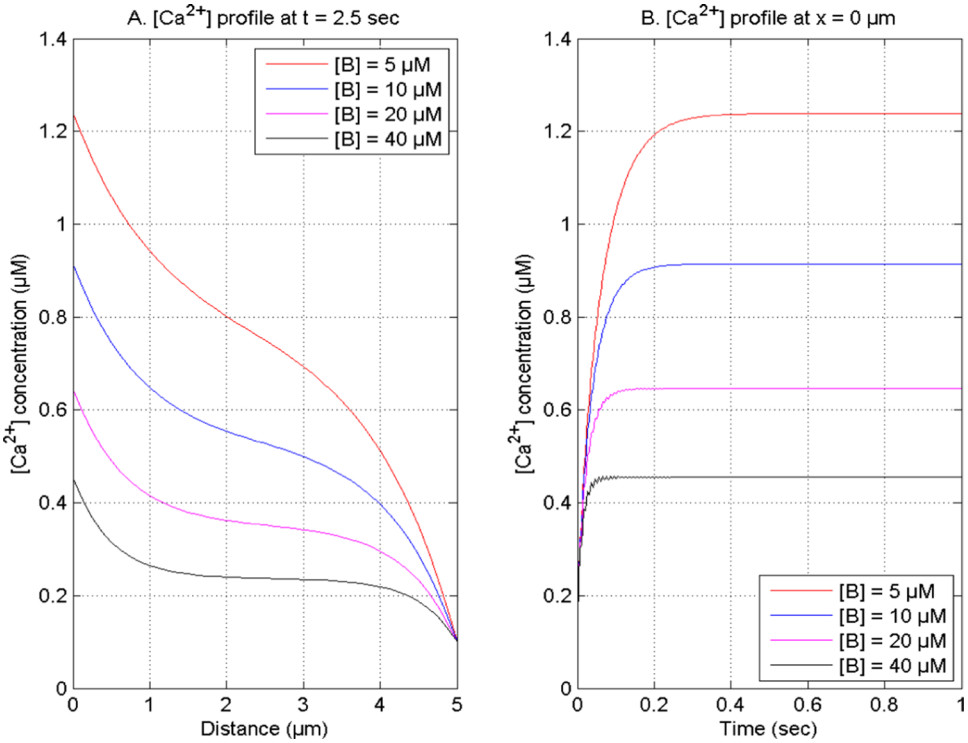

Fig. 5 [Ca^{2+}] concentration with VGCC, NCX, source influx (15 pA) and different buffer concentration amounts for time (2.5 s) and location (0 μm)

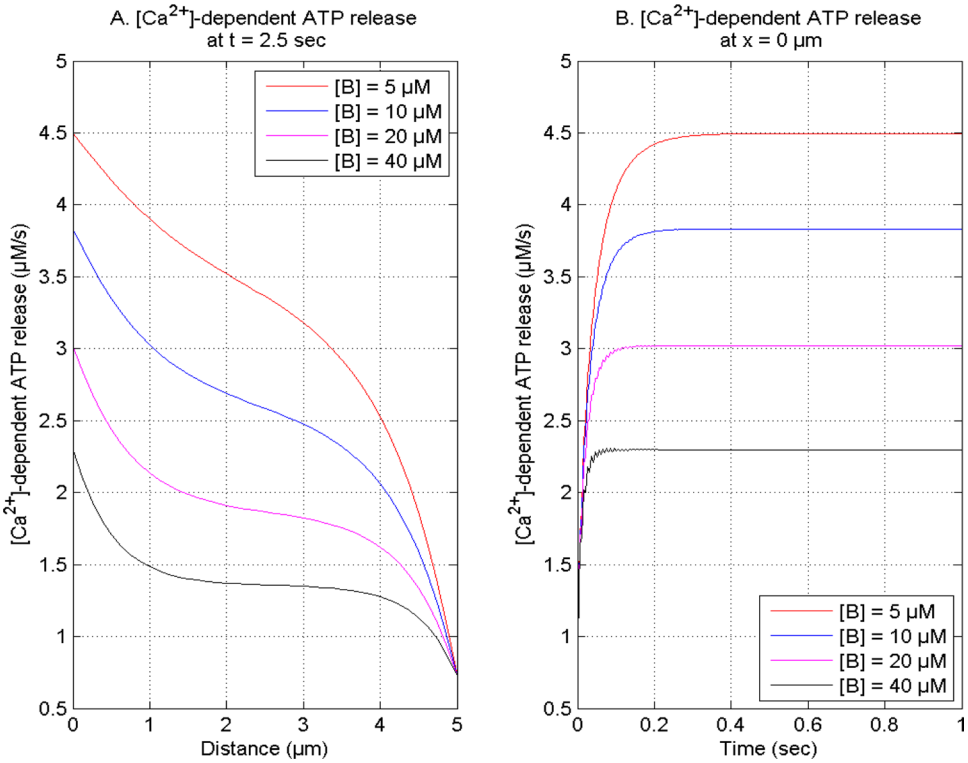

Fig. 6 [Ca^{2+}]-dependent ATP release with VGCC, NCX, σ = 15 pA and different buffer amounts at time (2.5 s) and location (0 μm)

The same behavior is noticed for ATP release in Fig. 7A, B for higher buffer concentration in neurons as the consequence of the influence of higher buffer on [Ca^{2+}] distribution is transferred to the ATP release via calcium signaling in neurons. Further, the steady-state achieved by [Ca^{2+}] and [Ca^{2+}]-dependent ATP release in Fig. 7 is almost near 0.3 s inspite of fluctuations created by higher buffer values. This indicates the capacity of the calcium control mechanism of

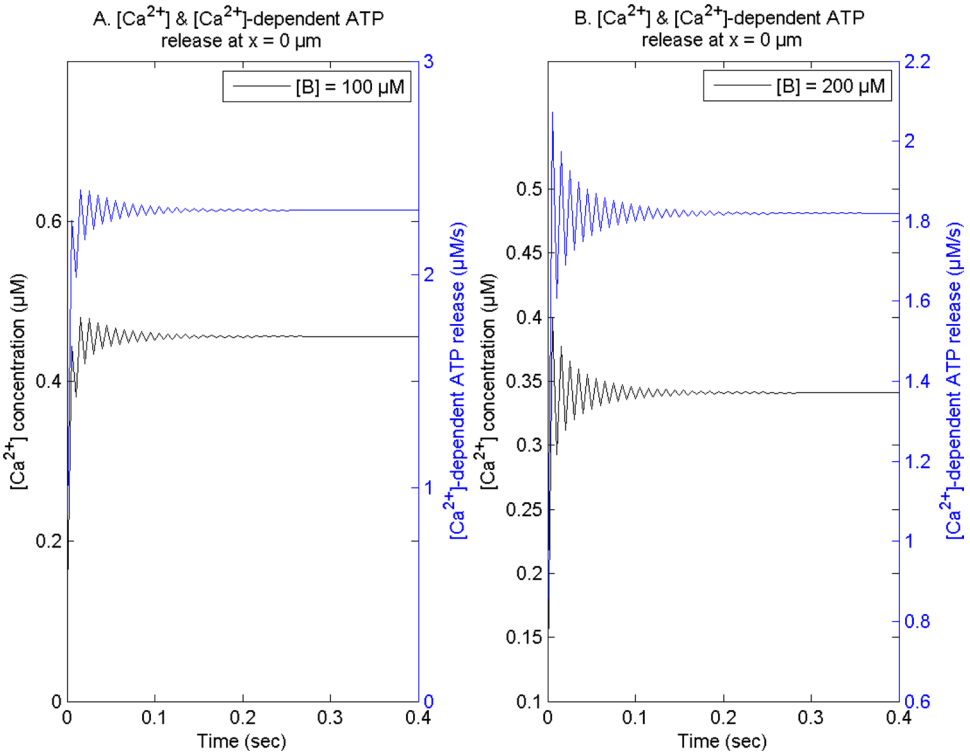

Fig. 7 [Ca^{2+}] and [Ca^{2+}]-dependent ATP release with VGCC and without NCX for σ = 15 pA and different buffer concentrations at location (0 μm). The scale and the curve of one colour are for [Ca^{2+}] and another scale and colour are for ATP release, respectively

the cell to neutralize the disturbances caused by any processes such as buffer etc. at the earliest possible time. The oscillations could be explained as a periodic adjustment of [Ca^{2+}] with the buffer concentrations, SERCA, and ER-mediated by IP_3R's.

Figure 8 demonstrates the source influx effects on the [Ca^{2+}] signaling and [Ca^{2+}]-associate ATP release at location $x = 0$ μm and t = 2.5 s in neurons. The source inflow is the crucial process for raising or reducing the [Ca^{2+}] distribution profile in the cytosol of nerve cells. When the source inflow amount elevates, the [Ca^{2+}] also increases in the ratio of increase in the source inflow. The same impact of source inflow on the calcium profile observed in Fig. 8A, C is also visible in Fig. 8B, D on ATP release. Thus, the regulation of [Ca^{2+}] and ATP release at required level in nerve cells can be achieved by the addition or reduction of the source influx.

Figure 9 displays the SERCA pump impacts on the [Ca^{2+}] concentrations at time 2.5 s and position of 0 μm in neurons. The [Ca^{2+}] concentration attains a high amount when SERCA pump is inactive, but when the pump rate becomes higher, the [Ca^{2+}] levels in the cytosol falls down. This is because the SERCA pumps out additional [Ca^{2+}] ions present in the cytosol into ER to keep the equitable concentrations of free cytosolic [Ca^{2+}] for the conventional functioning of the cell.

For time 2.5 s and position 2.5 μm, the Fig. 10 displays the SERCA pump's influence in [Ca^{2+}]-dependent release of ATP in nerve cells. The elevation in the values of V_SERCA begins with a reduction in calcium concentration because the SERCA pump is removing the cytosolic [Ca^{2+}] ions in neuron cells. Thus SERCA pump activity influences the ATP release by maintaining the low cytosolic [Ca^{2+}] level in nerve cells. The variations in the nonlinear behavior of the curves are due to the fact that at a higher SERCA pump rate, the calcium-reducing mechanisms have slight domination over calcium-elevating mechanisms and at a lower SERCA pump rate, the calcium-elevating mechanisms start dominating over calcium-reducing mechanisms in cells. Thus, the decrease in SERCA pump rate also decreases the nonlinear behavior of [Ca^{2+}]-dependent ATP release by elevating neuronal [Ca^{2+}] levels and higher ATP release in cells as illustrated in Fig. 10A. Thus, the elevation in the ATP release in the same proportion of elevation in [Ca^{2+}] levels due to a decrease in SERCA pump rate is observed during Ischemia in neuron cells.

The IP_3-receptor and the ryanodine receptor are functionally associated to trigger the CICR in neurons. The IP_3-induced [Ca^{2+}] release via IP_3-receptor elevates the cytosolic [Ca^{2+}] levels in neurons. The released calcium ions activate the adjacent ryanodine receptor, which further starts releasing high amounts of calcium ions along with IP_3R from ER to the cytosol through the CICR mechanism in cells. The impact of the ryanodine receptor on the [Ca^{2+}] distribution for normal and Ischemic neurons is depicted in Fig. 11 at time 2.5 s and position 2.5 μm. During Ischemia, the ryanodine receptor causes the higher cytosolic calcium

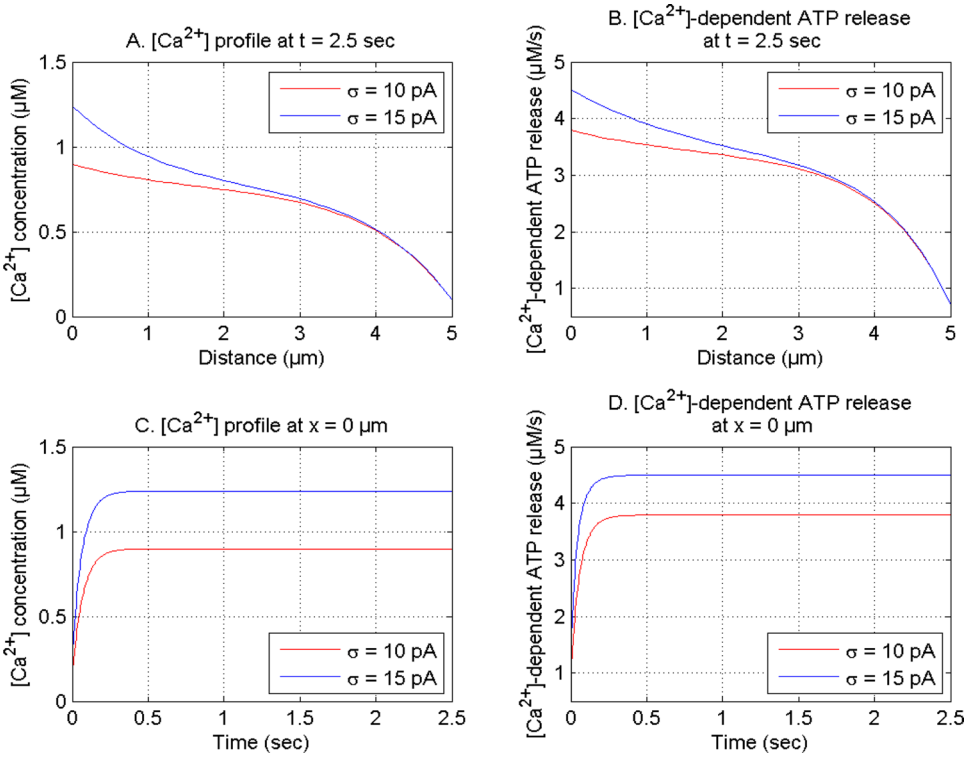

Fig. 8 [Ca^{2+}] and [Ca^{2+}]-dependent ATP release with VGCC, NCX, [B] = 5 μM for distinct [Ca^{2+}] source inflow amounts at location (0 μm) and time (2.5 s)

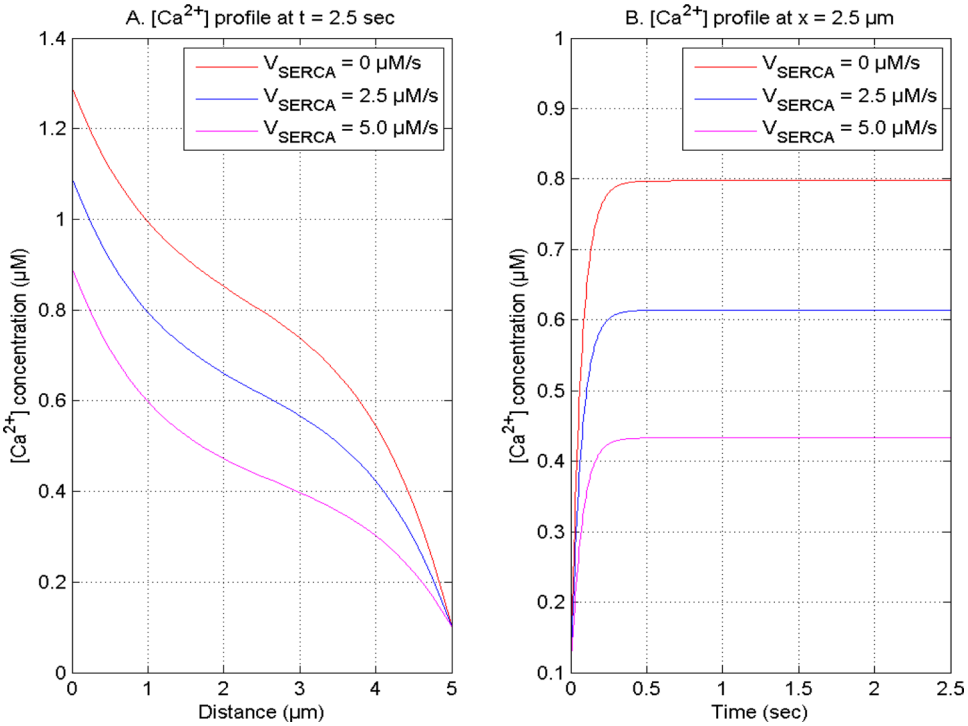

Fig. 9 [Ca^{2+}] profile with VGCC, NCX, σ = 15 pA & [B] = 5 μM for different SERCA pump rates at time (2.5 s) and location (0 μm)

concentration by aberrant [Ca^{2+}] ions release from ER in neuron cells than the normal neurons case. In Fig. 11, the [Ca^{2+}] concentration is high with the fully open state ($P_0 = 1.0$) of the RyR than the partially ($P_0 = 0.5$) or entirely ($P_0 = 0$) closed states of the RyR. As mentioned in the discussion of Fig. 10, similarly, the variations in the nonlinear behavior of [Ca^{2+}] are noted due to the variations in the [Ca^{2+}]-induced release of [Ca^{2+}] from the ER to the cytosol

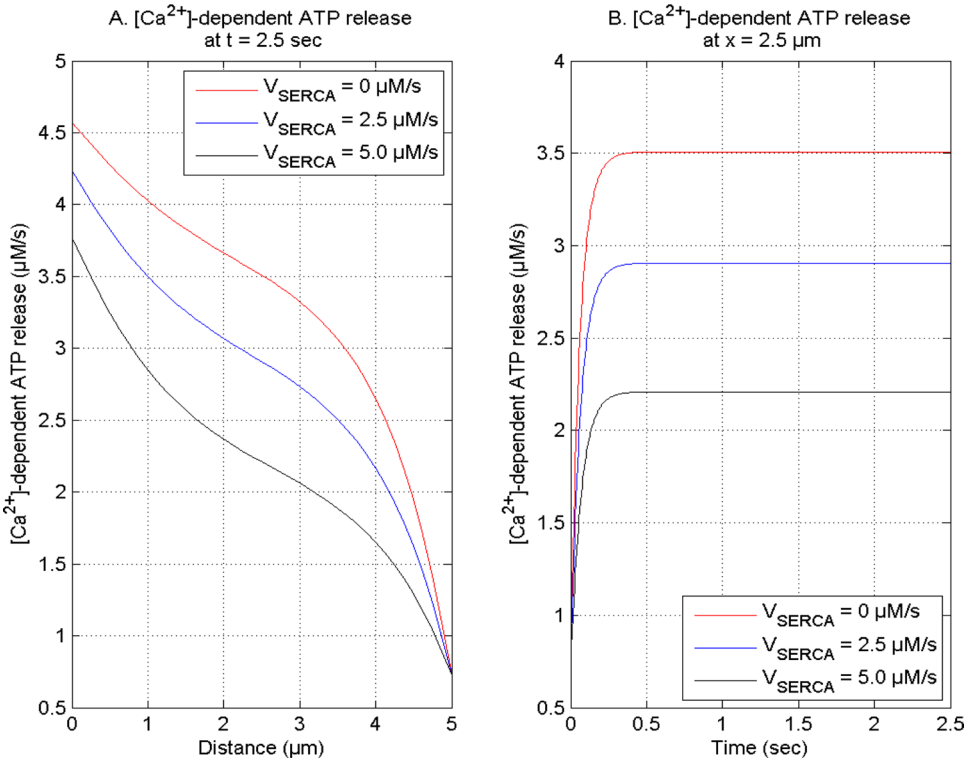

Fig. 10 [Ca^{2+}] profile with VGCC, NCX, [B] = 5 μM & σ = 15 pA for different SERCA pump rates at time (2.5 s) and location (2.5 μm)

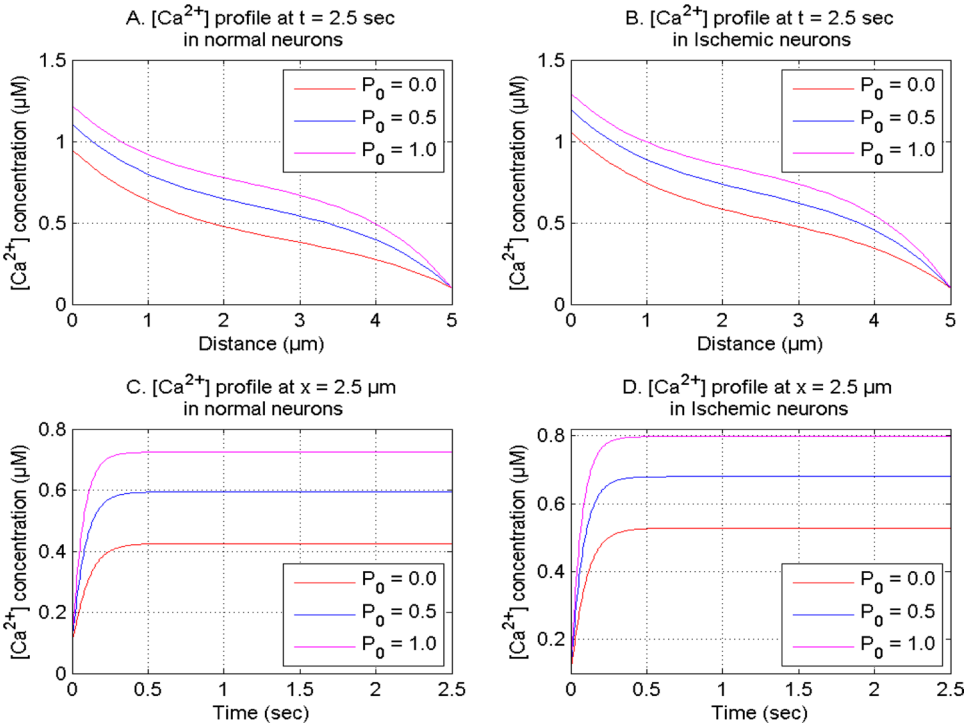

Fig. 11 [Ca^{2+}] concentration with VGCC, NCX, σ = 15 pA & [B] = 5 μM and different ryanodine receptor states at time (2.5 s) and location (2.5 μm)

of neurons for different RyR states as exhibited in Fig. 11A, B. Generally, the P_0 is, respectively, 0.5 and 1.0 in normal and Ischemic neurons. In Fig. 11A–D, for same value of P_0, the calcium concentration is slightly higher in Ischemic neurons as compared to that in normal neurons. However, if a general case is considered then the calcium concentration in Ischemic neurons ($P_0 = 1.0$) is much higher than that in normal neuron cells ($P_0 = 0.5$). Thus, dysregulation in the

ryanodine receptor may cause the elevation in $[Ca^{2+}]$ concentration during Ischemia in neuron cells.

The impacts of the CICR through the RyR on the $[Ca^{2+}]$-dependent ATP release in normal and Ischemic neuron cells are illustrated in Fig. 12 for time 2.5 s and location 2.5 µm. In the entirely open ryanodine receptor state ($P_0 = 1.0$), the $[Ca^{2+}]$-dependent ATP release is more elevated as compared to the partially ($P_0 = 0.5$) or completely ($P_0 = 0$) closed RyR's states in neuron cells. The behavior of spatial $[Ca^{2+}]$-dependent ATP-release curves also changes in the response to changes in the spatial calcium concentration curves for different RyR states in neurons. In Fig. 12A–D, for same value of P_0, the ATP release is slightly higher in Ischemic neurons as compared to that in normal neurons. However, if a general case is considered then the ATP release in Ischemic neurons ($P_0 = 1.0$) is much higher than that in normal neuron cells ($P_0 = 0.5$). Thus, the ryanodine receptor has a notable role in the ATP release during Ischemia in neuron cells.

The $[Ca^{2+}]$ concentration and flux of $[Ca^{2+}]$-dependent ATP release for normal, Ischemic, and Alzheimeric neuron cells are depicted in Fig. 13 for time $t = 2.5$ s. In the case of Alzheimeric neuron cells, there is more elevation in the $[Ca^{2+}]$ concentration as compared to the normal and Ischemic neuron cells since Alzheimer's patients have decreased calmodulin buffer amounts and buffer affinity in neuron cells (Dave and Jha 2018). Also, the $[Ca^{2+}]$ levels are higher in the Ischemic neuron cells than the normal neuron cells. Since the calcium release from the different channels including ryanodine receptor, IP_3 receptor, calcium source influx etc. are highly sensitive during Ischemia in contrast to the normal neuron cells. Similarly, the more elevated profiles of $[Ca^{2+}]$ and ATP release are noticed in the Alzheimeric neurons case since the elevation in the ATP release occurs in response to the increase in calcium levels in neurons. Also, the increased ATP release is observed in Ischemic neurons in comparison with normal neurons case. Thus, this indicates that the Ischemia-affected neurons may elevate the risk of neurons becoming Alzheimeric cells and the variations in the $[Ca^{2+}]$ concentration due to the normal, Ischemic, and Alzheimeric neurons are correlated with ATP release in neuron cells.

The effects of IP_3-receptor (IP_3R) on neuronal calcium and IP_3 profiles are exhibited in Fig. 14 at distinct times and sites. The spatiotemporal neuronal calcium concentration increases in the existence of IP_3R and decreases in the absence of IP_3R. The IP_3-induced calcium ions release through IP_3-receptor from ER to the cytosol elevates the cytosolic calcium concentration in neuron cells. The different IP_3R states also cause the changes in the IP_3 concentration in neurons. In Fig. 14C, the difference curves of spatial IP_3 for different IP_3R states increase with time and approach peak concentration nearer the centre of cells because of the fixed boundary concentration in neurons. For distinct IP_3R states, the difference curves of temporal IP_3 elevates with time for different locations in neurons as illustrated in Fig. 14D. Thus, the IP_3-receptor regulates the neuronal calcium and IP_3 concentration at appropriate levels and during

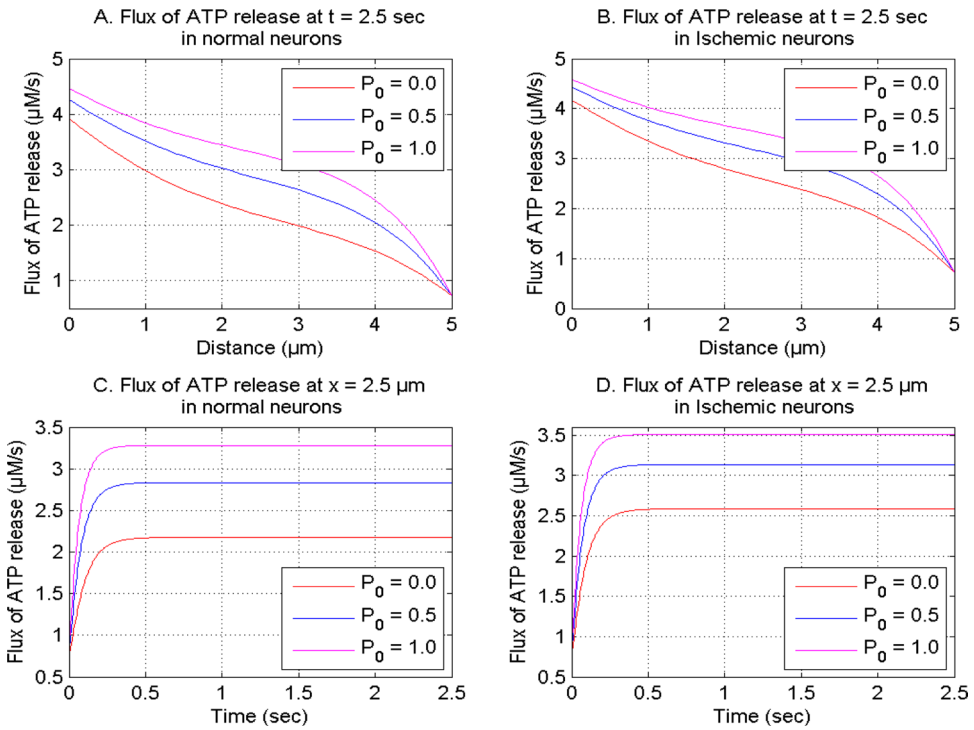

Fig. 12 $[Ca^{2+}]$-dependent ATP release with VGCC, NCX, $[B] = 5$ µM and $\sigma = 15$ pA for time (2.5 s) and site (2.5 µm)

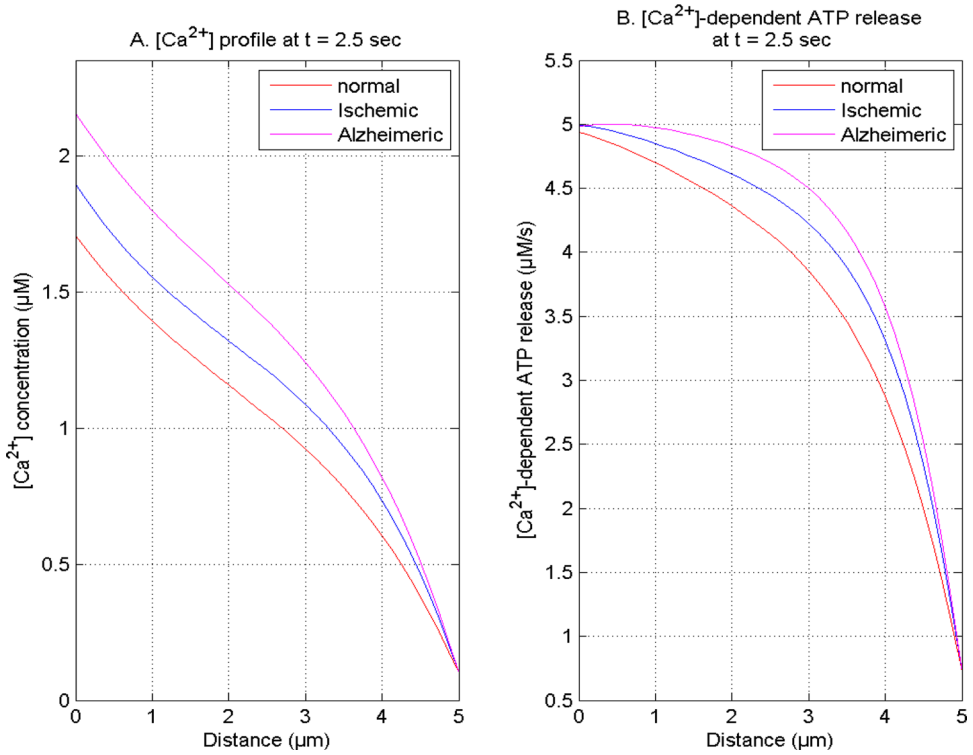

Fig. 13 [Ca^{2+}] and [Ca^{2+}]-dependent ATP release at time (0.5 s) and location (2.5 μm) for normal, Ischemic and Alzheimeric neuron cells

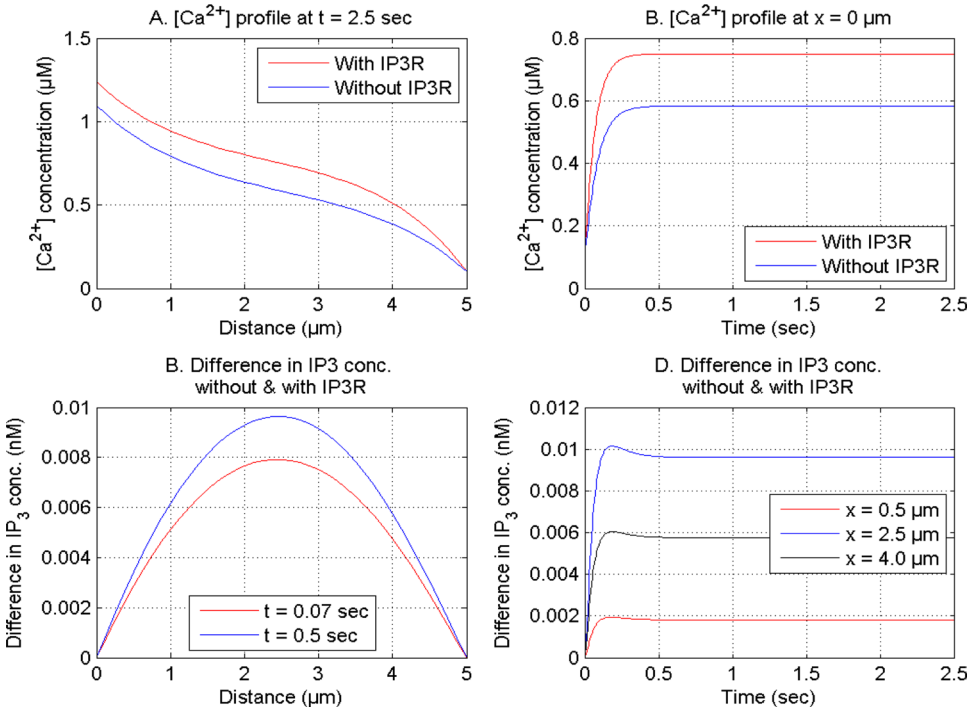

Fig. 14 [Ca^{2+}] concentration and difference in IP_3 concentration at distinct times and positions when IP_3-receptor is active and inactive

Ischemia, it causes the aberrant calcium ions release from ER to the cytosol of neurons.

The effects of sodium-calcium exchanger (NCX) in the presence of VGCC on the neuronal [Ca^{2+}] and ATP release are exhibited in Fig. 15 at time 2.5 s and position 0 μm. The NCX causes the extrusion of cytosolic [Ca^{2+}] ions, resulting in a reduction in the spatiotemporal [Ca^{2+}] levels and ATP release in neuron cells. Thus, NCX can play crucial role in regulating the appropriate calcium levels and ATP release in neuron cells. Any alteration in the activities of the NCX may cause the neurotoxicity in the form of different neurological disorders.

The errors have been computed and displayed in Tables 2 and 3 for $[Ca^{2+}]$ and IP_3 distribution, respectively. N is a number of elements. For t = 0.1, 0.2, 0.5, and 2.5 s, the model's accuracy for $[Ca^{2+}]$ is correspondingly 99.52%, 99.71%, 99.938708%, and 99.977781% and for IP_3 distribution, the accuracy is sequentially 99.96849%., 99.967305%, 99.97149%, and 99.989296%. Thus, the minimum accuracy and maximum error for $[Ca^{2+}]$ and IP_3 are, respectively, 99.52% and 0.48%. There is negligible grid sensitivity and this signifies the grid-independent solution.

The spectral radius (SR) was computed for stability analysis. If the SR is lesser or equal to one, the system is considered stable (Öziş et al. 2003). In the current condition, the SR was 0.9963, which is lesser to one. Thus, the FEM utilized in the current condition is stable.

For validation, the data provided in Table 4 for $[Ca^{2+}]$ and IP_3 concentrations have been calculated for Fig. 3 of Wagner et al. (2004) for the time 50 s and distance 1500 µm. Our outcomes for $[Ca^{2+}]$ and IP_3 concentrations were compared with the data provided in Table 4 for Wagner et al. (2004). The root mean square errors (RSME) have been computed between earlier results and current results and those are 0.0249 and 0.000028831, respectively, for $[Ca^{2+}]$ and IP_3, which are negligible. Also, the chi-square test has been conducted to determine whether the difference between the present findings and earlier published findings for calcium

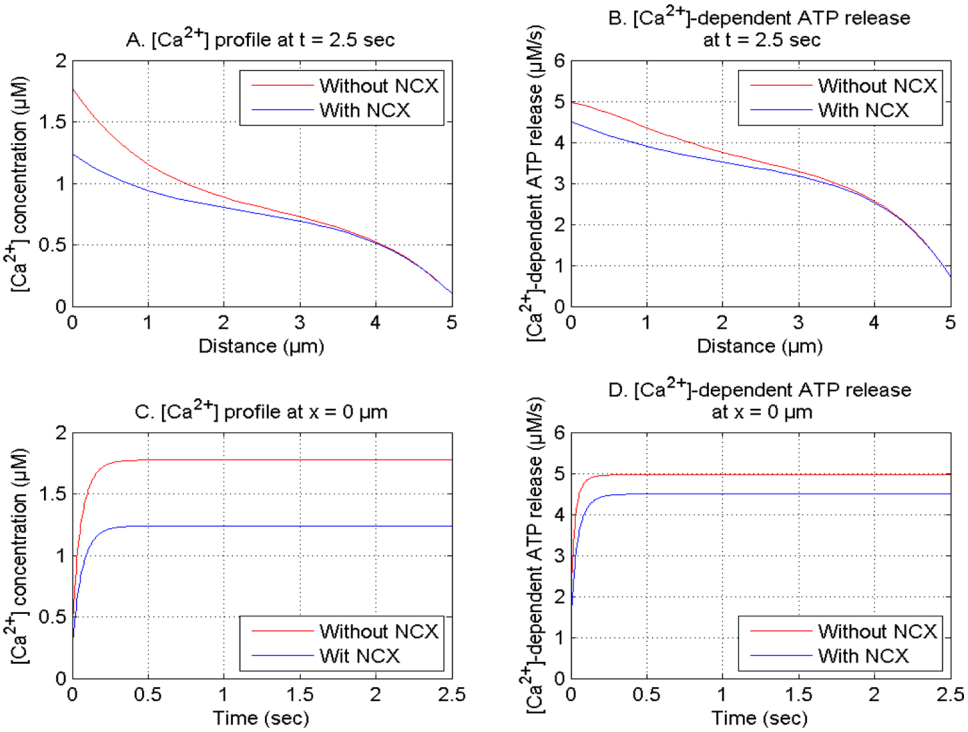

Fig. 15 $[Ca^{2+}]$ and $[Ca^{2+}]$-dependent ATP release with VGCC, buffer of 5 µM and source inflow at location (0 µm) and time (2.5 s) for different NCX states

Table 2 The errors in $[Ca^{2+}]$ distribution at location $x = 0$ µm

Time (sec)	$N = 40$	$N = 80$	Error	Error %
0.1	1.477165664802784	1.470055436314718	0.0071	0.48
0.2	1.685225751925853	1.680327464795490	0.0049	0.29
0.5	1.744912657791004	1.743843162979897	0.0011	0.061292
2.5	1.745643381837321	1.746031331648293	0.00038795	0.022219

Table 3 The errors in IP_3 distribution at location $x = 0.125$ µm

Time (sec)	$N = 40$	$N = 80$	Error	Error %
0.1	2.945878589775751	2.944950330001227	0.00092826	0.031510
0.2	2.937391226901331	2.936430857046460	0.00096037	0.032695
0.5	2.931604714062756	2.930768915184770	0.00083580	0.028510
2.5	2.929007443205269	2.928693920551353	0.00031352	0.010704

Table 4 $[Ca^{2+}]$ and IP_3 distribution compared with Wagner et al. (2004) at time 50 s.

Position (μm)	$[Ca^{2+}]$ concentration (Wagner et al. 2004)	$[Ca^{2+}]$ concentration (present outcomes)	IP_3 concentration (Wagner et al. 2004)	IP_3 concentration (present outcomes)
0	1.35000000000000	1.350000000000000	0.500000000000000	0.50000000000000
5	0.997185664535479	1.015874898040190	0.415142836839152	0.415113731789639
10	0.909668203960663	0.939502092653225	0.339171183581932	0.339119228995195
500	0.906155018029233	0.936612868374292	0.148912416500383	0.148832038039828
1500	0.100000000000000	0.100000000000000	0.160000000000000	0.160000000000000

and IP_3 concentration is statistically significant or not. For calcium and IP_3 concentrations, the chi-square values are, respectively, 0.00001685 and 8.5330×10^{-10}, which are less than the chi-square critical value. This implies that our null hypothesis that data and our results agree is true. Thus, our findings are in agreement with the outcomes of Wagner et al. (2004). The obtained outcomes are consistent with biological facts. However, no experimental findings are noted for the conditions of the present study for validation.

Conclusion

The finite element method with Crank–Nicholson procedure employed in the proposed model is quite flexible and very effective in generating mechanistic insights of the neurodynamics of interdependent calcium and IP_3 signaling processes and their impact on ATP release during Ischemia in neurons, which further leads to the condition of Alzheimer's-affected neurons.

One of the conclusions of our results confirms that the calcium concentration levels and ATP release are higher during Ischemia in neuron cells as reported by various researchers (Kalaria 2000; Volonté et al. 2003; Koistinaho and Koistinaho 2005; Wojda et al. 2008; Bodalia et al. 2013; Brini et al. 2014; Chung et al. 2015). The novel conclusions are the events and the factors leading to such high levels of $[Ca^{2+}]$ and ATP release in Ischemic neurons and are summarized below.

i. The higher amount of the source influx during Ischemia causes the increase in calcium concentration, which may further cause the higher ATP release in neurons. Any alteration in the source influx mechanism during Ischemia may lead to the condition of the Alzheimer's-affected neurons.
ii. The lower amount of SERCA pump rate enhances the $[Ca^{2+}]$ levels in neurons during Ischemia, and in response of the elevated $[Ca^{2+}]$ levels, the massive ATP release can occur in the Ischemic neurons. Also, the dysregulation of the SERCA mechanism is linked with Alzheimer's illness. The alteration in the extrusion of cytosolic $[Ca^{2+}]$ ions to ER in the Ischemic neurons can cause Alzheimer's disease.
iii. The lower amounts of the buffer increase the $[Ca^{2+}]$ concentration, which can cause higher ATP release during Ischemia in neuron cells. The disturbances in the buffer process in the Ischemic neurons may be responsible for Alzheimer's disorder.
iv. The higher buffer concentration causes disturbances in calcium concentration in the initial period of time, which may result in disturbances in the ATP release in the neuron cells during Ischemia. The dysregulation in the buffer mechanism can lead to the case of Alzheimer's-affected neurons.
v. The ryanodine receptor is highly sensitive in Ischemic neurons, which alters the ER mechanism and releases the $[Ca^{2+}]$ from ER to cytosol. The elevation in $[Ca^{2+}]$ concentration due to the dysregulation in the ryanodine receptor mechanism causes higher ATP release in the cell during Ischemia. Thus, the alteration in the ryanodine receptor mechanism may promote the condition from the Ischemic neurons to Alzheimer's-affected neurons.
vi. The Alzheimeric neuron cells have elevated profiles of $[Ca^{2+}]$ concentration and ATP release as compared to the Ischemia affected and normal neurons due to the association of calmodulin buffer with Alzheimer's patients.
vii. The alterations in calcium concentration due to the dysregulation in different mechanisms such as IP_3 receptor, ryanodine receptor, buffer, etc. can cause the disturbances in IP_3 concentration in Ischemic neurons, which may further lead to the alterations in IP_3-dependent ATP release in the cell.
viii. The elevation in $[Ca^{2+}]$ concentration in the existence of VGCC and absence of NCX dysregulates the IP_3 levels and ATP release in Ischemic neurons and develops the condition of Alzheimeric neurons.

Thus, one may conclude the above-mentioned events and factors can lead to the disturbances in the control mechanism of $[Ca^{2+}]$ and IP_3 dynamics in neuron cells. These may lead to the disturbances in release of the $[Ca^{2+}]$-dependent and IP_3-dependent ATP release in neurons during Ischemia.

Also, the Ischemic neurons can increase the possibility of Alzheimer's.

The findings of the present work provide the unexplored research direction in the field of computational neuroscience as well as establishes the basis for the further study of multisystem interactions of calcium and IP_3 with other systems including ATP, nitric oxide, β-amyloid, etc. in neuron cells during health and disease conditions. The results of such studies in future will be useful for biomedical scientists for the development of the diagnostic and therapeutic protocols.

The authors aim to extend the present model for the interactions of three system dynamics of calcium, IP_3, and ATP in the future to examine the mutual regulation and dysregulation of different dynamics on each other concerning normal and disease-affected neuron cells.

Appendix: Model equations summary

The FEM is a numerical-cum-analytical technique for solving boundary value problems. It involves the discretization of the domain into a finite number of sub-regions and then the solution of each sub-region is obtained by substituting an interpolation function. The solution of each sub-region is assembled to obtain the solution for the whole region. Here, Galerkin's approach is used to obtain the variational form. The unsteady state models of $[Ca^{2+}]$ and IP_3 diffusion concerning the one-dimensional case in neuron cells are constructed. The present problem is to get the solutions of Eq. (7) coupled with Eqs. (23, 25 and 26) concerning $[Ca^{2+}]$ and Eq. (17) coupled with Eqs. (24, 27 and 28) concerning IP_3. The length of the region is considered to be 5 µm, and divided into 40 elements from the source location to 5 µm. The initial and boundary conditions were constructed in light of biophysical conditions. The model equations for $[Ca^{2+}]$ and IP_3 dynamics are transformed into the variational form and Galerkin's finite element procedure was utilized to get the solution. Conveniently, the notations 'u' and 'v' are used instead of $[Ca^{2+}]$ and IP_3 and $e = 1, 2, 3, \ldots, 40$. Also, e depicts the e^{th} element and x_i and x_{i+1} depict the initial and terminal nodes of the e^{th} element.

For $[Ca^{2+}]$ and IP_3 distribution, shape functions for each element is considered as,

$$u^{(e)} = q_1^{(e)} + q_2^{(e)}\, x \tag{32}$$

$$v^{(e)} = r_1^{(e)} + r_2^{(e)}\, x \tag{33}$$

$$u^{(e)} = S^T q^{(e)},\ v^{(e)} = S^T r^{(e)} \tag{34}$$

$$S^T = [\,1\ \ x\,],\ q^{(e)^T} = [\,q_1^{(e)}\ \ q_2^{(e)}\,],\ r^{(e)^T} = [\,r_1^{(e)}\ \ r_2^{(e)}\,] \tag{35}$$

Putting nodal conditions in Eq. (34),

$$\overline{u}^{(e)} = S^{(e)} q^{(e)}, \overline{v}^{(e)} = S^{(e)} r^{(e)}, \tag{36}$$

where,

$$\overline{u}^{(e)} = \begin{bmatrix} u_i \\ u_j \end{bmatrix}, \overline{v}^{(e)} = \begin{bmatrix} v_i \\ v_j \end{bmatrix} \text{and} S^{(e)} = \begin{bmatrix} 1 & x_i \\ 1 & x_j \end{bmatrix} \tag{37}$$

From Eq. (36), we get

$$q^{(e)} = R^{(e)}\, \overline{u}^{(e)},\ r^{(e)} = R^{(e)}\, \overline{v}^{(e)} \tag{38}$$

And

$$R^{(e)} = S^{(e)^{-1}} \tag{39}$$

Substituting $q^{(e)}$ and $r^{(e)}$ from Eq. (38) in (34),

$$u^{(e)} = S^T\, R^{(e)} \overline{u}^{(e)},\ v^{(e)} = S^T\, R^{(e)} \overline{v}^{(e)} \tag{40}$$

The integrals $I_1^{(e)}$ and $I_2^{(e)}$ represent discretized variational forms of Eqs. (7) and (17). These forms are given below;

$$I_1^{(e)} = I_{a1}^{(e)} - I_{b1}^{(e)} + I_{c1}^{(e)} - I_{d1}^{(e)} + I_{e1}^{(e)} + I_{f1}^{(e)} - I_{g1}^{(e)} + I_{h1}^{(e)} - I_{i1}^{(e)} \tag{41}$$

where

$$I_{a1}^{(e)} = \int_{x_i}^{x_j} \left\{ \left(\frac{\partial u^{(e)}}{\partial x} \right)^2 \right\} dx \tag{42}$$

$$I_{b1}^{(e)} = \frac{d}{dt} \int_{x_i}^{x_j} \left[\frac{(u^{(e)})}{D_{Ca}} \right] dx \tag{43}$$

$$I_{c1}^{(e)} = \frac{V_{IPR}}{D_{ca} F_c} \int_{x_i}^{x_j} \left[\alpha_1 u^{(e)} + \alpha_2 v^{(e)} + \alpha_3 \right] dx \tag{44}$$

$$I_{d1}^{(e)} = \frac{V_{SERCA}}{D_{ca} F_c} \int_{x_i}^{x_j} \left[\beta_1 u^{(e)} + \beta_2 \right] dx \tag{45}$$

$$I_{e1}^{(e)} = \frac{V_{LEAK}}{D_{ca} F_c} \int_{x_i}^{x_j} \left[[Ca^{2+}]_{ER} - u^{(e)} \right] dx \tag{46}$$

$$I_{f1}^{(e)} = \frac{V_{RyR} P_0}{D_{ca} F_c} \int_{x_i}^{x_j} \left[[Ca^{2+}]_{ER} - u^{(e)} \right] dx \tag{47}$$

$$I_{g1}^{(e)} = \frac{K^+}{D_{ca}} \int_{x_i}^{x_j} \left[u^{(e)} - [Ca^{2+}]_\infty \right] dx \tag{48}$$

$$I_{h1}^{(e)} = \frac{1}{D_{ca}} \int_{x_i}^{x_j} \left[\theta_1 u^{(e)} - \theta_2 \right] dx \tag{49}$$

$$I_{i1}^{(e)} = f^{(e)} \left(\frac{\sigma_{Ca}}{D_{ca}} - \frac{\sigma_{NCX}}{D_{ca}} \right)_{x=0} \tag{50}$$

$$I_2^{(e)} = I_{a2}^{(e)} - I_{b2}^{(e)} + I_{c2}^{(e)} - I_{d2}^{(e)} \tag{51}$$

$$I_{a2}^{(e)} = \int_{x_i}^{x_j} \left\{ \left(\frac{\partial v^{(e)}}{\partial x} \right)^2 \right\} dx \tag{52}$$

$$I_{b2}^{(e)} = \frac{d}{dt} \int_{x_i}^{x_j} \left[\frac{v^{(e)}}{D_i} \right] dx \tag{53}$$

$$I_{c2}^{(e)} = \frac{V_{PROD}}{D_i F_c} \int_{x_i}^{x_j} \left[\mu_1 u^{(e)} + \mu_2 \right] dx \tag{54}$$

$$I_{d2}^{(e)} = \frac{\lambda}{F_c D_i} \int_{x_i}^{x_j} \left[\delta_1 u^{(e)} + \delta_2 v^{(e)} + \delta_3 \right] dx \tag{55}$$

The various coefficients α_1, α_2, α_3, β_1, β_2, θ_1, θ_2, μ_1, μ_2, δ_1, δ_2, and, δ_3 are determined by the linearization procedure for nonlinear terms of $[Ca^{2+}]$ and IP_3 distributions. The boundary conditions are incorporated in the analyzed equations to provide the system of equations as follows.

$$\frac{dI_1}{d\overline{u}^{(e)}} = \sum_{e=1}^{N} \overline{Q}^{(e)} \frac{dI_1^{(e)}}{d\overline{u}^{(e)}} \overline{Q}^{(e)^T} = 0 \tag{56}$$

$$\frac{dI_2}{d\overline{v}^{(e)}} = \sum_{e=1}^{N} \overline{Q}^{(e)} \frac{dI_2^{(e)}}{d\overline{v}^{(e)}} \overline{Q}^{(e)^T} = 0 \tag{57}$$

where,

$$\overline{Q}^{(e)} = \begin{bmatrix} 0 & 0 \\ . & . \\ 0 & 0 \\ 1 & 0 \\ 0 & 1 \\ 0 & 0 \\ . & . \\ 0 & 0 \end{bmatrix} \text{ and } \overline{u} = \begin{bmatrix} u_1 \\ u_2 \\ u_3 \\ . \\ . \\ u_{39} \\ u_{40} \\ u_{41} \end{bmatrix}, \overline{v} = \begin{bmatrix} v_1 \\ v_2 \\ v_3 \\ . \\ . \\ v_{39} \\ v_{40} \\ v_{41} \end{bmatrix} \tag{58}$$

$$\frac{dI_1^{(e)}}{d\overline{u}^{(e)}} = \frac{dI_{a1}^{(e)}}{d\overline{u}^{(e)}} + \frac{d}{dt}\frac{dI_{b1}^{(e)}}{d\overline{u}^{(e)}} + \frac{dI_{c1}^{(e)}}{d\overline{u}^{(e)}} - \frac{dI_{d1}^{(e)}}{d\overline{u}^{(e)}} + \frac{dI_{e1}^{(e)}}{d\overline{u}^{(e)}} + \frac{dI_{f1}^{(e)}}{d\overline{u}^{(e)}} - \frac{dI_{g1}^{(e)}}{d\overline{u}^{(e)}} + \frac{dI_{h1}^{(e)}}{d\overline{u}^{(e)}} - \frac{dI_{i1}^{(e)}}{d\overline{u}^{(e)}} \tag{59}$$

$$\frac{dI_2^{(e)}}{d\overline{v}^{(e)}} = \frac{dI_{a2}^{(e)}}{d\overline{v}^{(e)}} + \frac{d}{dt}\frac{dI_{b2}^{(e)}}{d\overline{v}^{(e)}} + \frac{dI_{c2}^{(e)}}{d\overline{v}^{(e)}} - \frac{dI_{d2}^{(e)}}{d\overline{v}^{(e)}} \tag{60}$$

$$[A]_{82\times82} \begin{bmatrix} \left[\frac{\partial \overline{u}}{\partial t}\right]_{41\times1} \\ \left[\frac{\partial \overline{v}}{\partial t}\right]_{41\times1} \end{bmatrix} + [B]_{82\times82} \begin{bmatrix} [\overline{u}]_{41\times1} \\ [\overline{v}]_{41\times1} \end{bmatrix} = [F]_{82\times1} \tag{61}$$

Here, A and B are system matrices with F as system vectors. The numerically stable Crank–Nicolson technique is utilized in FEM for time derivatives solution.

Author contributions We both authors contributed equally to this paper in terms of problem formulation, solution, data correction/literature review, and interpretation of the findings. Author (1) developed the Matlab program.

Funding Not Available.

Data availability Not Applicable.

Declarations

Conflict of interest The authors of this work state that they have no competing interests.

Ethical approval Not Applicable.

References

Ahmed Z, Connor JA (1988) Calcium regulation by and buffer capacity of molluscan neurons during calcium transients. Cell Calcium 9:57–69. https://doi.org/10.1016/0143-4160(88)90025-5

Allbritton NL, Meyer T, Stryer L (1992) Range of messenger action of calcium ion and inositol 1,4,5-trisphosphate. Science 258(80):1812–1815. https://doi.org/10.1126/science.1465619

Atri A, Amundson J, Clapham D, Sneyd J (1993) A single-pool model for intracellular calcium oscillations and waves in the Xenopus laevis oocyte. Biophys J 65:1727–1739. https://doi.org/10.1016/S0006-3495(93)81191-3

Berridge MJ, Irvine RF (1984) Inositol trisphosphate, a novel second messenger in cellular signal transduction. Nature 312:315–321. https://doi.org/10.1038/312315a0

Berridge MJ, Lipp P, Bootman MD (2000) The versatility and universality of calcium signalling. Nat Rev Mol Cell Biol 11(1):11–21. https://doi.org/10.1038/35036035

Bezprozvanny I, Watras J, Ehrlich BE (1991) Bell-shaped calcium-response curves of Ins(1,4,5)P_3- and calcium-gated channels from endoplasmic reticulum of cerebellum. Nature 351:751–754. https://doi.org/10.1038/351751a0

Bodalia A, Li H, Jackson MF (2013) Loss of endoplasmic reticulum Ca^{2+} homeostasis: contribution to neuronal cell death during cerebral ischemia. Acta Pharmacol Sin 34:49–59. https://doi.org/10.1038/aps.2012.139

Bootman MD, Berridge MJ (1995) The elemental principles of calcium signaling. Cell 83:675–678. https://doi.org/10.1016/0092-8674(95)90179-5

Brini M, Calì T, Ottolini D, Carafoli E (2014) Neuronal calcium signaling: function and dysfunction. Cell Mol Life Sci 71:2787–2814. https://doi.org/10.1007/s00018-013-1550-7

Brown SA, Morgan F, Watras J, Loew LM (2008) Analysis of phosphatidylinositol-4,5-bisphosphate signaling in cerebellar Purkinje spines. Biophys J 95:1795–1812. https://doi.org/10.1529/biophysj.108.130195

Bugrim A, Fontanilla R, Eutenier BB et al (2003) Sperm initiate a Ca^{2+} wave in frog eggs that is more similar to Ca^{2+} waves initiated by IP_3 than by Ca^{2+}. Biophys J 84:1580–1590. https://doi.org/10.1016/S0006-3495(03)74968-6

Bull R, Finkelstein JP, Gálvez J et al (2008) Ischemia enhances activation by Ca^{2+} and redox modification of ryanodine receptor channels from rat brain cortex. J Neurosci 28:9463–9472. https://doi.org/10.1523/JNEUROSCI.2286-08.2008

Choi DW (1988) Calcium-mediated neurotoxicity: relationship to specific channel types and role in ischemic damage. Trends Neurosci 11:465–469. https://doi.org/10.1016/0166-2236(88)90200-7

Chung JW, Ryu WS, Kim BJ, Yoon BW (2015) Elevated calcium after acute ischemic stroke: association with a poor short-term outcome and long-term mortality. J Stroke 17:54–59. https://doi.org/10.5853/jos.2015.17.1.54

Crank J (1979) The mathematics of diffusion. Oxford University Press, Ely House

Dave DD, Jha BK (2018) Delineation of calcium diffusion in Alzheimeric brain. J Mech Med Biol 18:1–15. https://doi.org/10.1142/S0219519418500288

Dave DD, Jha BK (2021) 2D finite element estimation of calcium diffusion in Alzheimer's affected neuron. Netw Model Anal Heal Inf Bioinform 10:1–11. https://doi.org/10.1007/s13721-021-00322-6

Deshpande JK, Siesjo BK, Wieloch T (1987) Calcium accumulation and neuronal damage in the rat hippocampus following cerebral ischemia. J Cereb Blood Flow Metab 7:89–95. https://doi.org/10.1038/jcbfm.1987.13

Falcke M (2003) Buffers and oscillations in intracellular Ca^{2+} dynamics. Biophys J 84:28–41. https://doi.org/10.1016/S0006-3495(03)74830-9

Falcke M, Huerta R, Rabinovich MI et al (2000) Modeling observed chaotic oscillations in bursting neurons: the role of calcium dynamics and IP_3. Biol Cybern 82:517–527. https://doi.org/10.1007/s004220050604

Fink CC, Slepchenko B, Moraru II et al (2000) An image-based model of calcium waves in differentiated neuroblastoma cells. Biophys J 79:163–183. https://doi.org/10.1016/S0006-3495(00)76281-3

Fogelson AL, Zucker RS (1985) Presynaptic calcium diffusion from various arrays of single channels. Implications for transmitter release and synaptic facilitation. Biophys J 48:1003–1017. https://doi.org/10.1016/S0006-3495(85)83863-7

Jagtap YD, Adlakha N (2018) Simulation of buffered advection diffusion of calcium in a hepatocyte cell. Math Biol Bioinform 13:609–619. https://doi.org/10.17537/2018.13.609

Jagtap Y, Adlakha N (2019) Numerical study of one-dimensional buffered advection–diffusion of calcium and IP_3 in a hepatocyte cell. Netw Model Anal Heal Inf Bioinform 8:1–9. https://doi.org/10.1007/s13721-019-0205-5

Jha A, Adlakha N (2015) Two-dimensional finite element model to study unsteady state Ca^{2+} diffusion in neuron involving ER LEAK and SERCA. Int J Biomath. https://doi.org/10.1142/S1793524515500023

Jha BK, Adlakha N, Mehta MN (2013) Two-dimensional finite element model to study calcium distribution in astrocytes in presence of VGCC and excess buffer. Int J Model Simul Sci Comput. https://doi.org/10.1142/S1793962312500304

Jha BK, Adlakha N, Mehta MN (2014) Two-dimensional finite element model to study calcium distribution in astrocytes in presence of excess buffer. Int J Biomath 7:1–11. https://doi.org/10.1142/S1793524514500314

Kalaria RN (2000) The role of cerebral ischemia in Alzheimer's disease. Neurobiol Aging 21:321–330. https://doi.org/10.1016/S0197-4580(00)00125-1

Keener J, Sneyd J (2009) Mathematical physiology, 2nd edn. Springer, New York. https://doi.org/10.1007/978-0-387-75847-3

Keizer J, De Young G (1993) Effect of voltage-gated plasma membrane Ca^{2+} fluxes on IP_3-linked Ca^{2+} oscillations. Cell Calcium 14:397–410. https://doi.org/10.1016/0143-4160(93)90044-7

Koistinaho M, Koistinaho J (2005) Interactions between Alzheimer's disease and cerebral ischemia—focus on inflammation. Brain Res Rev 48:240–250. https://doi.org/10.1016/j.brainresrev.2004.12.014

Kotwani M, Adlakha N, Mehta MN (2012) Numerical model to study calcium diffusion in fibroblasts cell for one dimensional unsteady state case. Appl Math Sci 6:5063–5072

Kotwani M, Adlakha N, Mehta MN (2014) Finite element model to study the effect of buffers, source amplitude and source geometry on spatiooral calcium distribution in fibroblast cell. J Med Imaging Heal Inf 4:840–847. https://doi.org/10.1166/jmihi.2014.1328

Li YX, Rinzel J (1994) Equations for $InsP_3$ receptor-mediated [Ca^{2+}] (i) oscillations derived from a detailed kinetic model: a hodgkin-huxley like formalism. J Theor Biol 166:461–473. https://doi.org/10.1006/jtbi.1994.1041

Llinas R (1979) The role of calcium in neuronal function. Neurosci Fourth Study Progr 51:555–571

Manhas N, Anbazhagan N (2021) A mathematical model of intricate calcium dynamics and modulation of calcium signalling by mitochondria in pancreatic acinar cells. Chaos Solitons Fractals 145:9–12. https://doi.org/10.1016/j.chaos.2021.110741

Manhas N, Pardasani KR (2014) Mathematical model to study IP_3 dynamics dependent calcium oscillations in pancreatic acinar cells. J Med Imaging Heal Inf 4:874–880. https://doi.org/10.1166/jmihi.2014.1333

Manhas N, Sneyd J, Pardasani KR (2014) Modelling the transition from simple to complex Ca^{2+}oscillations in pancreatic acinar cells. J Biosci 39:463–484. https://doi.org/10.1007/s12038-014-9430-3

Mattson MP, Zhu H, Yu J, Kindy MS (2000) Presenilin-1 mutation increases neuronal vulnerability to focal ischemia in vivo and to hypoxia and glucose deprivation in cell culture: Involvement of

perturbed calcium homeostasis. J Neurosci 20:1358–1364. https://doi.org/10.1523/jneurosci.20-04-01358.2000
Michell RH (1975) Inositol phospholipids and cell surface receptor function. BBA Rev Biomembr 415:81–147. https://doi.org/10.1016/0304-4157(75)90017-9
Naik PA, Pardasani KR (2015) One dimensional finite element model to study calcium distribution in oocytes in presence of VGCC, RyR and buffers. J Med Imaging Heal Inf 5:471–476. https://doi.org/10.1166/jmihi.2015.1431
Naik PA, Pardasani KR (2016) Finite element model to study calcium distribution in oocytes involving voltage gated Ca^{2+} channel, ryanodine receptor and buffers. Alexandria J Med 52:43–49. https://doi.org/10.1016/j.ajme.2015.02.002
Naik PA, Pardasani KR (2019) Three-dimensional finite element model to study effect of RyR calcium channel, ER leak and SERCA pump on calcium distribution in oocyte cell. Int J Comput Methods 16:1–19. https://doi.org/10.1142/S0219876218500913
Nelson DL, Cox MM (2005) Lehninger principles of biochemistry, 4th edn. WH Freeman and Company, New York
Öziş T, Aksan EN, Özdeş A (2003) A finite element approach for solution of Burgers' equation. Appl Math Comput 139:417–428. https://doi.org/10.1016/S0096-3003(02)00204-7
Panday S, Pardasani KR (2013) Finite element model to study effect of advection diffusion and Na^{+}/Ca^{2+} exchanger on Ca^{2+} distribution in oocytes. J Med Imaging Heal Inf 3:374–379. https://doi.org/10.1166/jmihi.2013.1184
Pathak KB, Adlakha N (2015) Finite element model to study calcium signalling in cardiac myocytes involving pump, leak and excess buffer. J Med Imaging Heal Inf 5:683–688. https://doi.org/10.1166/jmihi.2015.1443
Pathak K, Adlakha N (2016) Finite element model to study two dimensional unsteady state calcium distribution in cardiac myocytes. Alexandria J Med 52:261–268. https://doi.org/10.1016/j.ajme.2015.09.007
Pawar A, Pardasani KR (2022a) Effect of disturbances in neuronal calcium and IP_3 dynamics on β-amyloid production and degradation. Cogn Neurodyn 2022:1–18. https://doi.org/10.1007/S11571-022-09815-0
Pawar A, Pardasani KR (2022b) Simulation of disturbances in interdependent calcium and β-amyloid dynamics in the nerve cell. Eur Phys J Plus 1378(137):1–23. https://doi.org/10.1140/EPJP/S13360-022-03164-X
Pawar A, Pardasani KR (2022c) Study of disorders in regulatory spatiotemporal neurodynamics of calcium and nitric oxide. Cogn Neurodyn. https://doi.org/10.1007/s11571-022-09902-2
Pawar A, Pardasani KR (2022d) Effects of disorders in interdependent calcium and IP_3 dynamics on nitric oxide production in a neuron cell. Eur Phys J Plus 137:543. https://doi.org/10.1140/EPJP/S13360-022-02743-2
Pawar A, Pardasani KR (2023) Computational model of calcium dynamics-dependent dopamine regulation and dysregulation in a dopaminergic neuron cell. Eur Phys J Plus 123:1–19. https://doi.org/10.1140/epjp/s13360-023-03691-1
Pluta R, Jabłoński M, Ułamek-Kozioł M et al (2013) Sporadic Alzheimer's disease begins as episodes of brain ischemia and ischemically dysregulated alzheimer's disease genes. Mol Neurobiol 48:500–515. https://doi.org/10.1007/s12035-013-8439-1
Pluta R, Januszewski S, Czuczwar SJ (2021) Brain ischemia as a prelude to Alzheimer's disease. Front Aging Neurosci 13:1–12. https://doi.org/10.3389/fnagi.2021.636653
Rasmussen H, Barrett PQ (1984) Calcium messenger system: an integrated view. Physiol Rev 64:938–984. https://doi.org/10.1152/physrev.1984.64.3.938
Rossi DJ, Brady JD, Mohr C (2007) Astrocyte metabolism and signaling during brain ischemia. Nat Neurosci 10:1377–1386. https://doi.org/10.1038/nn2004
Ruiz A, Matute C, Alberdi E (2009) Endoplasmic reticulum Ca^{2+} release through ryanodine and IP_3 receptors contributes to neuronal excitotoxicity. Cell Calcium 46:273–281. https://doi.org/10.1016/j.ceca.2009.08.005
Siesjö BK (1984) Cell damage in the brain: a speculative synthesis. Acta Psychiatr Scand 70:57–91. https://doi.org/10.1111/j.1600-0447.1984.tb07154.x
Sims CE, Allbrittont NL (1998) Metabolism of inositol 1,4,5-trisphosphate and inositol 1,3,4,5- tetrakisphosphate by the oocytes of Xenopus laevis. J Biol Chem 273:4052–4058. https://doi.org/10.1074/jbc.273.7.4052
Singh N, Adlakha N (2019) Nonlinear dynamic modeling of 2-dimensional interdependent calcium and inositol 1,4,5-trisphosphate in cardiac myocyte. Math Biol Bioinform 14:290–305. https://doi.org/10.17537/2019.14.290
Singh N, Adlakha N (2020) Effect of source geometry on interdependent calcium and inositol 1; 4; 5-trisphosphate dynamics in a cardiac myocyte cell. Springer Proc Math Stat 308:75–83. https://doi.org/10.1007/978-981-15-1338-1_6
Smith GD (1996) Analytical steady-state solution to the rapid buffering approximation near an open Ca^{2+} channel. Biophys J 71:3064–3072. https://doi.org/10.1016/S0006-3495(96)79500-0
Smith GD, Wagner J, Keizer J (1996) Validity of the rapid buffering approximation near a point source of calcium ions. Biophys J 70:2527–2539. https://doi.org/10.1016/S0006-3495(96)79824-7
Stamatakis M, Mantzaris NV (2006) Modeling of ATP-mediated signal transduction and wave propagation in astrocytic cellular networks. J Theor Biol 241:649–668. https://doi.org/10.1016/j.jtbi.2006.01.002
Stutzmann GE, Mattson MP (2011) Endoplasmic reticulum Ca^{2+} handling in excitable cells in health and disease. Pharmacol Rev 63:700–727. https://doi.org/10.1124/pr.110.003814
Tewari S, Pardasani KR (2008) Finite difference model to study the effects of Na^{+} influx on cytosolic Ca^{2+} diffusion. World Acad Sci Eng Technol 2:670–675
Tewari SG, Pardasani KR (2010) Finite element model to study two dimensional unsteady state cytosolic calcium diffusion in presence of excess buffers. IAENG Int J Appl Math 40:1–5. https://www.iaeng.org/IJAM/issues_v40/issue_3
Tewari SG, Pardasani KR (2012) Modeling effect of sodium pump on calcium oscillations in neuron cells. J Multiscale Model 04:1250010. https://doi.org/10.1142/s1756973712500102
Tewari V, Tewari S, Pardasani KR (2011) A model to study the effect of excess buffers and Na + ions on Ca^{2+} diffusion in neuron cell. World Acad Sci Eng Technol 76:41–46. https://doi.org/10.5281/zenodo.1054988
Tripathi A, Adlakha N (2011) Closed form solution to problem of calcium diffusion in cylindrical shaped neuron cell. World Acad Sci Eng Technol 80:739–742. https://doi.org/10.5281/zenodo.1078819
Tripathi A, Adlakha N (2012) Two dimensional coaxial circular elements in FEM to study calcium diffusion in neuron cells. Appl Math Sci 6:455–466
Tymianski M, Tator C (1996) Normal and abnormal calcium homeostasis in neurons: a basis for the pathophysiology of traumatic and ischemic central nervous system injury. Neurosurgery 38:1176–1195. https://doi.org/10.1097/00006123-199606000-00028
Verkhratsky A (2002) The endoplasmic reticulum and neuronal calcium signalling. Cell Calcium 32:393–404. https://doi.org/10.1016/S0143416002001896
Volonté C, Amadio S, Cavaliere F et al (2003) Extracellular ATP and neurodegeneration. Curr Drug Targets CNS Neurol Disord 2:403–412. https://doi.org/10.2174/1568007033482643
Wagner J, Keizer J (1994) Effects of rapid buffers on Ca^{2+} diffusion and Ca^{2+} oscillations. Biophys J 67:447–456. https://doi.org/10.1016/S0006-3495(94)80500-4

Wagner J, Fall CF, Hong F et al (2004) A wave of IP_3 production accompanies the fertilization Ca^{2+} wave in the egg of the frog, Xenopus laevis: theoretical and experimental support. Cell Calcium 35:433–447. https://doi.org/10.1016/j.ceca.2003.10.009

Wojda U, Salinska E, Kuznicki J (2008) Calcium ions in neuronal degeneration. IUBMB Life 60:575–590. https://doi.org/10.1002/iub.91

Yanagihara T, John TM (1982) Ionic shift in cerebral ischemia. Life Sci 30:1921–1925. https://doi.org/10.1016/0024-3205(82)90473-8